The Cosmic Microwave Background: State of the Art

R. Belén Barreiro [a,b,c]

[a] *Astrophysics Group, Cavendish Laboratory, Madingley Road Cambridge CB3 0HE, UK*

[b] *Instituto de Física de Cantabria, Facultad de Ciencias, Avda. de los Castros s/n 39005 Santander, Spain*

[c] *Depto. Física Moderna, Facultad de Ciencias, Avda. de los Castros s/n 39005 Santander, Spain*

We review the current status of the cosmic microwave background (CMB) radiation, including a brief discussion of some basic theoretical aspects as well as a summary of anisotropy detections and CMB experiments. We focus on the description of some relevant characteristics of the microwave foregrounds, on the discussion of the different estimators proposed in the literature to detect non-Gaussianity and on outlining the bases of different reconstruction methods that have been applied to the CMB.

Key words: Cosmic microwave background

1 Introduction

The Cosmic Microwave Background (CMB) Radiation constitutes one of the most powerful tools of Cosmology. This radiation is a relic from a hot and dense past of the universe, produced at the Big Bang and freely propagated ~ 300000 years after it. Before these early times, due to the high temperature, matter is completely ionized. Compton scattering tightly couples the photons to the electrons which are in turn coupled to the baryons by electromagnetic interactions. As the universe expands, the temperature decreases and at a redshift $z \sim 1000$, T has dropped to $\sim 3000K$, allowing free electrons and protons to form neutral atoms. At this time, known as *decoupling*, the universe becomes transparent, the photons are last scattered off by the electrons and can freely propagate, giving rise to the CMB. Due to the thermal equilibrium between matter and radiation before decoupling and their lack of interaction after that time, the CMB exhibits a blackbody spectrum with a present temperature of $T_o = 2.73K$. The temperature of the CMB has dropped since decoupling due

to the expansion of the universe according to $T(z) = (1+z)T_o$, where $T(z)$ denotes the temperature measured by an observer at redshift z.

The existence of the CMB was first predicted by Gamow and his collaborators in 1948, when studying the light-element synthesis in the primordial universe. They predicted that this relic radiation should still be ubiquitous today, with a temperature of about 5K (Gamow 1948a,b, Alpher & Herman 1948). It was not until 1964, when the discovery of the CMB was made by Penzias and Wilson (published in 1965). They detected an excess of noise in their horn antenna with a temperature $\sim 3K$ coming from all directions in the sky and being very uniform. For a historical introduction see Partridge (1995). The temperature of the CMB has been measured by the FIRAS instrument on board the COBE satellite to be $T_o = 2.728 \pm 0.004$K (Fixsen *et al.* 1996). The prediction and the subsequent detection of the CMB is one of the strongest supports for the Big Bang model.

Since the CMB freely propagated after the decoupling time, it carries information about how the universe was at $z \lesssim 1000$. The fact that the CMB is very homogeneous, means that so was the primitive universe. However, the matter in our universe clusters on a wide range of scales, forming all the structures we see today. If all these structures were formed via gravitational instability, those density fluctuations should already be present at early times, leaving their imprint as temperature anisotropies in the CMB.

2 Temperature anisotropies

The temperature anisotropies of the CMB are described by a 2-dimensional random field $\frac{\Delta T}{T}(\vec{n}) \equiv \frac{T(\vec{n})-T_o}{T_o}$, where $\vec{n}$ is a unit vector on the sphere. It is usual to expand the field in spherical harmonics:

$$\frac{\Delta T}{T}(\vec{n}) = \sum_{\ell=1}^{\infty} \sum_{m=-\ell}^{\ell} a_{\ell m} Y_{\ell m}(\vec{n}) \,, \tag{1}$$

In this expansion, low ℓ's correspond to anisotropies on large angular scales whereas large ℓ's reflect the anisotropies at small scales. The $a_{\ell m}$ coefficients are independent random variables of mean $< a_{\ell m} >= 0$. If the temperature fluctuations are *statistically* isotropic, the variance of the $a_{\ell m}$ coefficients is independent of m:

$$< a_{\ell m} a^*_{\ell' m'} >= C_\ell \delta_{\ell \ell'} \delta_{m m'} \,, \tag{2}$$

where the averages are to be taken over statistical ensembles. The set of C_ℓ's constitutes the *angular power spectrum*. In the case of Gaussian fluctuations, as predicted by inflation, the 2-point correlation function $C(\theta)$ completely characterizes the random temperature field and can be written as:

$$C(\theta) = \left\langle \left(\frac{\Delta T}{T}(\vec{n_1}) \cdot \frac{\Delta T}{T}(\vec{n_2}) \right) \right\rangle = \sum_\ell \frac{(2\ell+1)}{4\pi} C_\ell P_\ell \left(cos\theta\right) , \qquad (3)$$

where P_ℓ is the Legendre polynomial of order ℓ and θ is the angle formed by the vectors $\vec{n_1}$ and $\vec{n_2}$ on the sky. Therefore, for standard inflationary models, the angular power spectrum contains all the statistical information about the field, being the fundamental quantity in the theory of the CMB anisotropies. The C_ℓ's can be accurately calculated for the inflationary models as a function of the cosmological parameters (e.g. Seljak & Zaldarriaga 1996, Hu *et al.* 1998). Thus, accurate measurements of the angular power spectrum would provide tight constrains on the cosmological model (Bond *et al.* 1997). For theories generating non-Gaussian fluctuations, study of higher order moments becomes necessary. However, the angular power spectrum is still a fundamental test of the viability of those theories.

The accuracy with which a given C_ℓ can be measured is limited by the so-called *cosmic variance*, which is due to the fact of having just a single realization of the temperature field, our universe. For Gaussian fluctuations each C_ℓ is drawn from a χ^2 distribution with $(2\ell+1)$ degrees of freedom. The minimum variance of a measured C_ℓ is given by $[2/(2\ell+1)]C_\ell^2$, mainly affecting the low ℓ's (large scales). Another effect that reduces our ability to accurately measure the angular power spectrum is the *sample variance*, which is due to partial coverage of the sky. This effect enhances the cosmic variance by a factor $\simeq 4\pi/A$ where A is the solid angle covered by the experiment (Scott *et al.* 1994). Even full-sky coverage satellite missions can be affected by sample variance, since we may need to discard highly contaminated parts of the data (such as the Galactic plane) when studying the CMB. It must be pointed out that cosmic and sample variance are present independently of the resolution and sensitivity of the experiment.

3 Summary of anisotropy detections

Before COBE, the only temperature anisotropy detected in the CMB was of dipolar nature (Smoot *et al.* 1977). This dipolar component is the largest anisotropy present in the CMB and it is due to a Doppler shift caused by the motion of the observer with respect to the rest frame of the CMB (i.e., it has

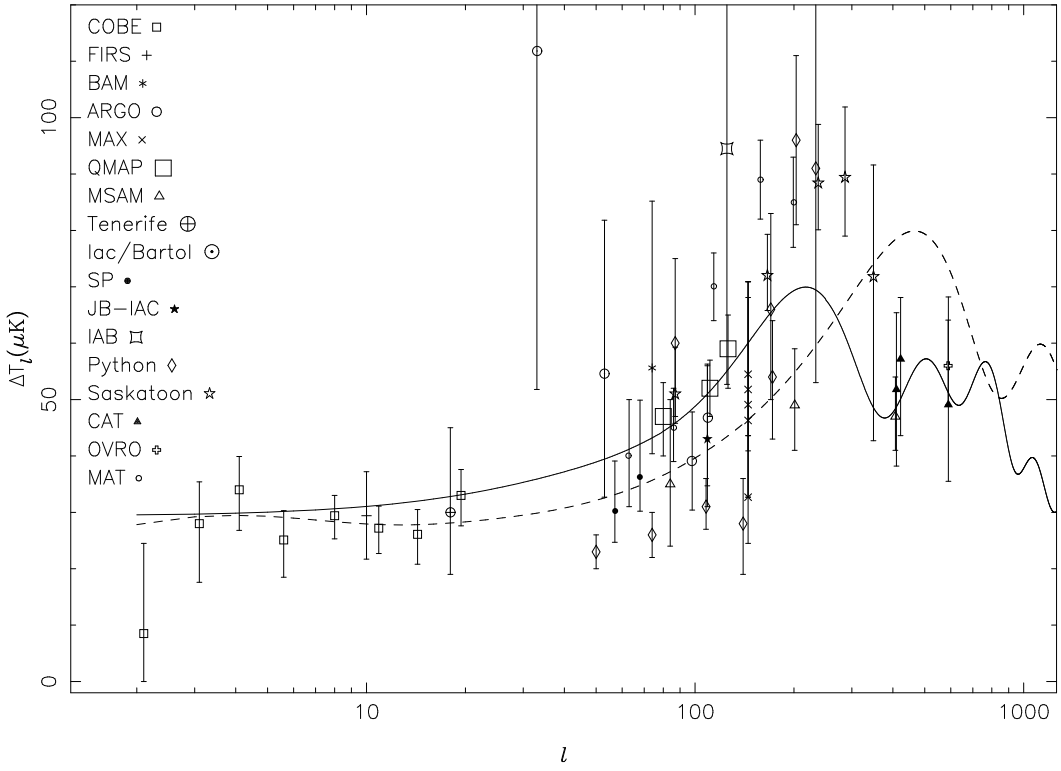

Fig. 1. Anisotropy detections in the CMB with the error bars showing the 1σ confidence level. The solid and dashed line correspond to the angular power spectrum predicted for a standard flat and open ($\Omega = 0.3$) CDM models, respectively.

an extrinsic origin):

$$T(\theta) \approx T_o(1 + (v/c)\cos\theta) \ , v/c << 1 \, , \tag{4}$$

where v is the velocity of the observer with respect to the CMB and θ the angle formed by the line of sight and the velocity. The COBE team found an amplitude for the dipole of 3.372 ± 0.007mK with a maximum in the direction $(\ell, b) = (264.14^\circ \pm 0.30^\circ, 48.26^\circ \pm 0.30^\circ)$ (Fixsen *et al.* 1996).

In 1992, the COBE team announced the first detection of intrinsic anisotropy of the CMB, at angular scales of $\sim 10^\circ$, at the level of $\sim 10^{-5}$ (Smoot *et al.* 1992). Since then, more than a dozen of groups have reported anisotropy detections spanning over many angular scales.

When observing the microwave sky, we must take into account the resolution, sensitivity and observing technique of the experiment. The sensitivity of the experiment to any given scale is defined by the window function W_ℓ (e.g. White & Srednicki 1994, Cayón 1996). For instance, for a Gaussian beam the window function is $W_\ell = e^{-\ell(\ell+1)^2\sigma_b^2}$, where σ_b is the dispersion of the beam. In addition, instrumental noise must be taken into account when interpreting the data. The temperature fluctuation averaged over the sky observed by an

Table 1
Summary of anisotropy detections by COBE and balloon-borne experiments

Experiment	$\Delta T_{\ell}{}^{+\sigma}_{-\sigma}(\mu K)$	ℓ_{min}	ℓ_{eff}	ℓ_{max}	Reference
COBE 1	$8.5^{+16.0}_{-8.5}$	2	2.1	2.5	Tegmark & Hamilton 1997
COBE 2	$28.0^{+7.4}_{-10.4}$	2.5	3.1	3.7	Tegmark & Hamilton 1997
COBE 3	$34.0^{+5.9}_{-7.2}$	3.4	4.1	4.8	Tegmark & Hamilton 1997
COBE 4	$25.1^{+5.2}_{-6.6}$	4.7	5.6	6.6	Tegmark & Hamilton 1997
COBE 5	$29.4^{+3.6}_{-4.1}$	6.8	8.0	9.3	Tegmark & Hamilton 1997
COBE 6	$27.7^{+3.9}_{-4.5}$	9.7	10.9	12.2	Tegmark & Hamilton 1997
COBE 7	$26.1^{+4.4}_{-5.3}$	12.8	14.3	15.7	Tegmark & Hamilton 1997
COBE 8	$33.0^{+4.6}_{-5.4}$	16.6	19.4	22.1	Tegmark & Hamilton 1997
FIRS	$29.4^{+7.8}_{-7.7}$	3	10	30	Ganga *et al.* 1994
BAM	$55.6^{+29.6}_{-15.2}$	28	74	97	Tucker *et al.* 1997
ARGO 1	$39.1^{+8.7}_{-8.7}$	52	98	176	de Bernardis *et al.* 1994
ARGO 2	$46.8^{+9.5}_{-12.1}$	53	109	179	Masi *et al.* 1996
MAX GUM	$54.5^{+16.4}_{-10.9}$	78	145	263	Tanaka *et al.* 1996
MAX ID	$46.3^{+21.8}_{-13.6}$	78	145	263	Tanaka *et al.* 1996
MAX SH	$49.1^{+21.8}_{-16.4}$	78	145	263	Tanaka *et al.* 1996
MAX HR	$32.7^{+10.9}_{-8.2}$	78	145	263	Tanaka *et al.* 1996
MAX PH	$51.8^{+19.1}_{-10.9}$	78	145	263	Tanaka *et al.* 1996
QMAP I+II	47^{+6}_{-7}	39	80	121	de Oliveira-Costa *et al.* 1998
QMAP I+II	59^{+6}_{-7}	72	126	180	de Oliveira-Costa *et al.* 1998
QMAP I+II	52^{+5}_{-5}	47	111	175	de Oliveira-Costa *et al.* 1998
MSAM I	35^{+15}_{-11}	39	84	130	Wilson *et al.* 1999
MSAM I	49^{+10}_{-8}	131	201	283	Wilson *et al.* 1999
MSAM I	47^{+7}_{-6}	284	407	453	Wilson *et al.* 1999

experiment is given by:

$$\left(\frac{\Delta T}{T}\right)^2_{rms} = \sum_{\ell} \frac{2\ell+1}{4\pi} C_{\ell} W_{\ell} \tag{5}$$

In order to compare the measured fluctuations from different experiments with the angular power spectrum predicted by the theory, the power per logarithmic scale $\left(\frac{\Delta T}{T}\right)^2_{\ell} \equiv \ell(\ell+1)C_{\ell}/(2\pi)$ is commonly used. Assuming that this quantity

Table 2
Summary of anisotropy detections by ground-based experiments

Experiment	$\Delta T_{\ell}{}^{+\sigma}_{-\sigma}(\mu K)$	ℓ_{min}	ℓ_{eff}	ℓ_{max}	Reference
Tenerife	30^{+15}_{-11}	11	18	27	Gutiérrez *et al.* 1999
IAC/Bartol 1	$111.8^{+65.4}_{-60.0}$	20	33	57	Femenia *et al.* 1998
IAC/Bartol 2	$54.5^{+27.3}_{-21.8}$	38	53	75	Femenia *et al.* 1998
SP91	$30.2^{+8.9}_{-5.5}$	31	57	106	Gundersen *et al.* 1995
SP94	$36.3^{+13.6}_{-6.1}$	36	68	106	Gundersen *et al.* 1995
JB-IAC	43^{+13}_{-12}	90	109	128	Dicker *et al.* 1999
IAB	$94.5^{+41.8}_{-41.8}$	60	125	205	Piccirillo & Calisse 1993
Python III	60^{+15}_{-13}	49	87	105	Platt *et al.* 1997
Python I+II+III	66^{+17}_{-16}	120	170	239	Platt *et al.* 1997
Python V	23^{+3}_{-3}	21	50	94	Coble *et al.* 1999
Python V	26^{+4}_{-4}	35	74	130	Coble *et al.* 1999
Python V	31^{+5}_{-4}	67	108	157	Coble *et al.* 1999
Python V	28^{+8}_{-9}	99	140	195	Coble *et al.* 1999
Python V	54^{+10}_{-11}	132	172	215	Coble *et al.* 1999
Python V	96^{+15}_{-15}	164	203	244	Coble *et al.* 1999
Python V	91^{+32}_{-38}	195	233	273	Coble *et al.* 1999
MAT	40^{+10}_{-9}	45	63	81	Torbet *et al.* 1999
MAT	45^{+7}_{-6}	64	86	102	Torbet *et al.* 1999
MAT	70^{+6}_{-6}	90	114	134	Torbet *et al.* 1999
MAT	89^{+7}_{-7}	135	158	180	Torbet *et al.* 1999
MAT	85^{+8}_{-8}	170	199	237	Torbet *et al.* 1999
Saskatoon 1 (*)	$51.0^{+8.3}_{-5.2}$	58	87	126	Netterfield *et al.* 1997
Saskatoon 2	$72.0^{+7.3}_{-6.2}$	123	166	196	Netterfield *et al.* 1997
Saskatoon 3	$88.4^{+10.4}_{-8.3}$	196	237	266	Netterfield *et al.* 1997
Saskatoon 4	$89.4^{+12.5}_{-10.4}$	248	286	310	Netterfield *et al.* 1997
Saskatoon 5	$71.8^{+19.8}_{-29.1}$	308	349	393	Netterfield *et al.* 1997
CAT 1	$51.8^{+13.6}_{-13.6}$	339	410	483	Scott *et al.* 1996
CAT 1	$49.1^{+19.1}_{-13.6}$	546	590	722	Scott *et al.* 1996
CAT 2	$57.2^{+10.9}_{-13.6}$		422		Baker *et al.* 1999
OVRO	$56^{+8.1}_{-6.9}$	361	589	756	Leitch *et al.* 1998

$*$ The Saskatoon data include the latest calibration correction (Leitch *et al.* 1998).

is flat over the range of multipoles where the experiment is more sensitive, it can be easily estimated from the measured temperature fluctuation $\left(\frac{\Delta T}{T}\right)_{rms}$ as (Bond 1995):

$$\left(\frac{\Delta T}{T}\right)_\ell^2 = \frac{\left(\frac{\Delta T}{T}\right)_{rms}^2}{\sum_\ell W_\ell \frac{2\ell+1}{2\ell(\ell+1)}}\,, \tag{6}$$

what is usually known as the *band power*.

In figure 1, a compilation of anisotropy detections is plotted, where the vertical error bars show the 1σ confidence level. Horizontal error bars, that account for the range of multipoles where the experiment is sensitive, are not plotted for the sake of clarity. The value of the detections and the 1σ error bars are listed in table 1 (from COBE and balloon-borne experiments) and 2 (from ground based experiments). ℓ_{eff} corresponds to the centre of the window function and ℓ_{min} and ℓ_{max} to the multipoles where it drops to half of its central value (except for COBE, where ℓ_{min} and ℓ_{max} indicate the rms width of the window function as calculated in Tegmark & Hamilton 1997). Part of these numbers have been taken from the compilations of Griffiths *et al.* (1999) and M.Tegmark's web page[1]. For comparison, the angular power spectrum for two standard CDM models ($H_0 = 50$, $\Omega_b = 0.05$ and initial scale invariant perturbations) with $\Omega = 1$ (solid line) and $\Omega = 0.3$ are also plotted (dashed line).

At large scales ($\ell \lesssim 20$), the data are consistent with a Harrison-Zel'dovich primordial spectrum $C_\ell \propto 1/(\ell(\ell+1))$ as predicted by inflation (see § 5). At medium angular scales, although the scatter is still large, the data seem to indicate the presence of a Doppler peak at $\ell \sim 200$. New data obtained from several experiments capable of measuring this range of ℓ's with good precision, such as Boomerang or Maxima, are currently under analysis and will confirm whether the first Doppler peak has been actually detected.

4 Summary of CMB experiments

During the last years, there has been an explosion of experiments dedicated to measure the CMB temperature anisotropies. Ground based, including interferometers, and balloon-borne experiments have been designed to probe a large range of angular scales. Two satellite missions have also been approved: the MAP satellite of the NASA and the Planck Mission of the ESA. The expected

[1] http://www.sns.ias.edu/∼max/#CMB

Table 3
Summary of ground based experiments

Experiment†	Resolution	Frequency (GHz)	Detectors
APACHE(c)	$30'$	90-259	Bol
ACBAR(p)	$\sim 5'$	150-450	Bol
ATCA(c)*	$2'$	8.7	HEMT
CAT(c)*	$10' - 30'$	13-17	HEMT
CBI(p)*	$4.5' - 10'$	26-36	HEMT
CG(c)	$\sim 1'$	1-32	HEMT
DASI(p)*	$0.25^\circ - 1.15^\circ$	26-36	HEMT
HACME/SP(f)	$46'$	39-43	HEMT
IAC/Bartol(f)	2°	91-272	Bol
JB-IAC(c)*	2°	33	HEMT
MAT(c)	$12'$	30-440	HEMT/SIS
OVRO 40/5(c)	$7' - 22'$	14.5-32	HEMT
Python(f)	$45'$	37-90	Bol/HEMT
Saskatoon(f)	$0.5^\circ - 1.5^\circ$	26-46	HEMT
SuZIE(c)	$\sim 2'$	143-350	Bol
Tenerife(c)	5°	10-33	HEMT
Viper(c)	$20' - 2'$	35-400	HEMT/Bol
VLA(f)*	$\sim 10''$	8.4	HEMT
VSA(p)*	$0.25^\circ - 2^\circ$	26-36	HEMT
White Dish(f)	$12'$	90	Bol

† An 'f' after the experiment's name means it's finished; a 'c' denotes current; a 'p' denotes planned.

∗ Interferometer

launch dates are 2001 and 2007, respectively. Both satellites will provide multifrequency full sky maps at unprecedented angular resolution and sensitivity.

A summary of recently completed, current and future experiments is given in tables 3 (ground-based) and 4 (balloon-borne). A list of the web sites related to these CMB experiments (including the satellite missions) is given after the bibliography. For a more detailed description of these experiments see the reviews of Halpern & Scott (1999), Smoot (1997), Lasenby *et al.* (1998) and de

Table 4
Summary of balloon-borne experiments

Experiment†	Resolution	Frequency (GHz)	Detectors
ACE(p)	$9'$	90	HEMT
Archeops(p)	$8', 5.5', 5'$	143-353	Bol
ARGO(f)	$52'$	150-600	Bol
BAM(c)	$42'$	93-276	Bol
BEAST(p)	$25', 19', 9'$	30-90	HEMT
BOOMERanG(c)	$20', 12'$	90-400	Bol
FIRS(f)	3.8°	170-680	Bol
MAX(f)	$30'$	105-420	Bol
MAXIMA(c)	$10'$	150-410	Bol
MSAM I(f)	$37'$	170-680	Bol
MSAM II(c)	$20'$	70-170	Bol
QMAP(f)	$54', 36'$	30-40	HEMT
TopHat(c)	$20'$	70-630	Bol

† An 'f' after the experiment's name means it's finished; a 'c' denotes current; a 'p' denotes planned.

Bernardis & Masi (1998). In addition, several experiments will measure the polarization of the microwave sky (see Staggs & Gundersen 1999 for a description). In Figure 2, kindly provided by M.Tegmark, the frequency-multipole range covered by various CMB experiments is given. The shaded regions indicate where the different foregrounds (see § 7) are expected to dominate over the cosmological signal.

MAP will measure the microwave sky in five different frequencies ranging $22 - 90$ GHz with a resolution $\sim 20'$ and a sensitivity of $35\mu K$ per $0.3^\circ \times 0.3^\circ$ pixel during one year of continuous observation. This sensitivity is expected to be increased to $\sim 20\mu K$ when combining the three highest frequency channels. This will allow to map the power spectrum up to ℓ's$\sim$ 800. In Table 5, the main characteristics of the MAP satellite are given.

The Planck satellite is constituted by two different instruments: the Low Frequency Instrument (LFI) and the High Frequency Instrument (HFI). The LFI will use HEMT technology and will measure the microwave sky at frequencies 30-100 GHz. The HFI will be based on bolometers and will cover frequencies from 100-900 GHz. Planck will provide multifrequency all-sky maps at a resolution $\sim 10'$ and a sensitivity $\frac{\Delta T}{T} \sim 2 \times 10^{-6}$. The characteristics of the

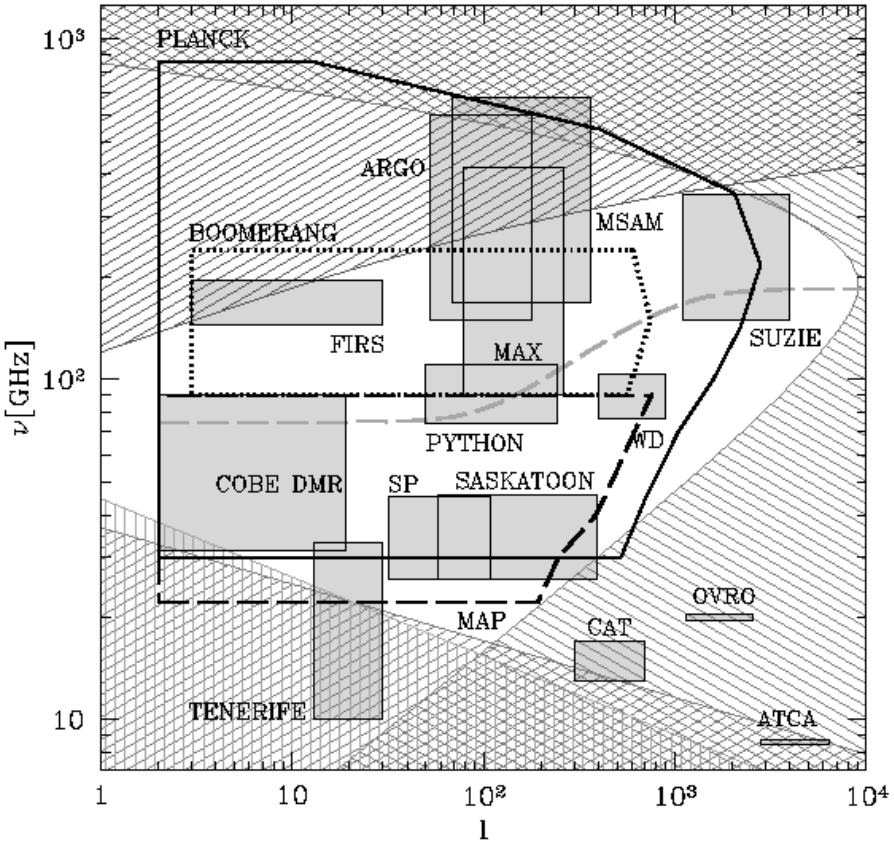

Fig. 2. The boxes indicate the frequency-multipole range probed by several CMB experiments. The shaded regions show where the foregrounds fluctuations are expected to exceed those of the cosmological signal in the cleanest 20% of the sky. They correspond to dust (top), free-free emission (lower left, vertically shaded), synchrotron(lower left) and point-sources (lower and upper right). The heavy dashed line shows where the total foreground contribution to each multipole is minimal. Figure kindly provided by M.Tegmark. .

proposed Planck payload are summarized in table 6 (Tauber 1999).

5 Initial density perturbations

The study of the CMB temperature anisotropies is tightly related to the initial matter density (scalar) perturbations. Initial vorticity (rotational) perturbations decay as the universe expands and, therefore, are not relevant. Initial gravitational wave (tensor) perturbations can leave their imprint in the CMB (we will comment about this in §6.2.1). According to the present theories of galaxy formation, all the structures of the universe would have formed from these initial density perturbations that eventually would have collapsed via

Table 5
MAP instrument description

Frequency (GHz)	Wavelength (mm)	FWHM	No. of channels	Sensitivity (μK) $0.3^\circ \times 0.3^\circ pixel$
22	13.6	0.93°	4	35
30	10.0	0.68°	4	35
40	7.5	0.47°	8	35
60	5.0	0.35°	8	35
90	3.3	0.21°	16	35

Table 6
Characteristics of proposed Planck payload

Inst.	Freq. (GHz)	Angular resolution	Detector technology	Detector temp.(K)	No. of detectors	Bandwidth ($\Delta\nu/\nu$)	Sensitivity*	Sensitive to linear pol.
LFI	30	$33'$	HEMT	~ 20	4	0.2	1.6	yes
LFI	44	$23'$	HEMT	~ 20	6	0.2	2.4	yes
LFI	70	$14'$	HEMT	~ 20	12	0.2	3.6	yes
LFI	100	$10'$	HEMT	~ 20	34	0.2	4.3	yes
HFI	100	$10.7'$	Bol	0.1	4	0.25	1.7	no
HFI	143	$8.0'$	Bol	0.1	12	0.25	2.0	yes
HFI	217	$5.5'$	Bol	0.1	12	0.25	4.3	yes
HFI	353	$5.0'$	Bol	0.1	6	0.25	14.4	no
HFI	545	$5.0'$	Bol	0.1	8	0.25	147.0	yes
HFI	857	$5.0'$	Bol	0.1	6	0.25	6670	no

$*$ Average $\frac{\Delta T}{T}$ per resolution element (12 months of observation, 1σ, $10^{-6} units$)

gravitational instability. There are two main scenarios that try to explain the formation of these initial seeds: inflation and topological defects.

In the inflationary paradigm (Guth 1982, Linde 1982,1983, Albrecht & Steinhardt 1982) these fluctuations are originated from quantum fluctuations which are boosted in scale during the exponential expansion that characterizes the inflationary epoch (Hawking 1982, Guth & Pi 1982, Starobinskii 1982, Bardeen *et al.* 1983). Inflation can also explain why the universe is so homogenous at large scale. Regions that appear today causally disconnected, were in causal contact before the exponential inflation. On the other hand, a flat universe arises naturally from inflation, which would explain why the value of Ω is so close to 1 at present. Standard inflation also predicts that the primordial density perturbations are a realization of a homogeneous and isotropic Gaussian random field, which leaves a Gaussian imprint in the CMB.

An alternative mechanism to induce initial perturbations are topological de-

fects, such as cosmic strings, textures and monopoles, which may form during symmetry breaking phase transitions in the early Universe (for a review see Vilenkin & Shellard 1994). An important property of the CMB temperature fluctuations induced by topological defects is their non-Gaussian character. Therefore, testing the Gaussianity of the CMB would allow to discriminate between the inflationary and topological defects scenarios.

However, appreciable deviation from non-Gaussianity can also arise in non-standard inflationary models (Salopek 1992, Peebles 1999a,b). On the other hand, hybrid scenarios that combine inflation and topological defects have also been proposed (Jeannerot 1996, Linde *et al.* 1997, Avelino *et al.* 1998).

Two different classes of initial density fluctuations are distinguished: *adiabatic* and *isocurvature*. The adiabatic fluctuations are characterised by a null fluctuation of specific entropy associated to each component $\delta\left(\frac{n_b}{n_\gamma}\right) = \delta\left(\frac{n_x}{n_\gamma}\right) = 0$ at each point, which implies the following relation at the initial time:

$$\delta_\gamma = \frac{4}{3}\delta_b = \frac{4}{3}\delta_X \tag{7}$$

where δ_γ, δ_b and δ_X denote the initial density fluctuations associated to photons, baryons and non-baryonic dark matter component, respectively. The isocurvature fluctuations are characterized by a null fluctuation of total energy at each point, i.e., $\delta(\rho_\gamma + \rho_b + \rho_X) = 0$, what keeps constant the space curvature. In addition it is usually assumed that the entropy per baryon remains constant, i.e. $\delta\left(\frac{n_b}{n_\gamma}\right) = 0$, when there exists a non-baryonic dark matter component. This leads to the following relation at the initial time:

$$\delta_\gamma = -\frac{4\rho_X}{3\rho_b + 4\rho_\gamma}\delta_X \tag{8}$$

The inflationary models favour adiabatic fluctuations (e.g. Kolb & Turner, 1990) with a Harrison-Zel'dovich spectrum (see below) but isocurvature fluctuations are also possible (Efstathiou & Bond 1986, Peebles 1999a,b).

In the case of Gaussian fluctuations, they are fully characterised by their power spectrum P(k). This quantity reflects how the amplitude of the fluctuation depends on the wavenumber k (or equivalently, on the scale):

$$P(k) = \left\langle |\delta(k)|^2 \right\rangle = Ak^n\,, \tag{9}$$

where $\delta(\vec{k})$ are the Fourier components of the density fluctuation field, A is a normalization constant and n is the spectral index. For the case of adiabatic fluctuations, $n = 1$ corresponds to the so-called Harrison-Zel'dovich (Harrison

1970, Zel'dovich 1972) or scale invariant spectrum. This scale invariance means that the amplitude of the density fluctuations is the same when it enters the horizon scale.

In addition to baryonic matter, non-baryonic *dark matter* is believed to be present in our universe. This idea is strongly supported by different observations (e.g. White *et al.* 1993, Tyson *et al.* 1998, see also van den Bergh 1999 and references therein). Two candidates for this kind of matter have been mainly considered. Cold dark matter (CDM) is constituted by weakly interacting particles whose velocity dispersion is negligible compared to that of galaxies at the epoch of galaxy formation, such as WIMP's (weakly interactive massive particles) or the axion. On the other hand, hot dark matter (HDM) is constituted by particles that keep relativistic up to recent times, such as light neutrinos with non-zero mass. We must point out that baryon perturbations evolve differently from perturbations in cold or hot dark matter.

6 Sources of temperature anisotropies

Density perturbations leave their imprint as temperature anisotropies in the CMB. Their statistical properties can be calculated for the inflationary paradigm with an accuracy better than 1% (e.g. Seljak & Zaldarriaga 1996, Hu *et al.* 1998). However, the situation becomes much more complicate for the topological defects scenarios due to the non-linear evolution of the defects and their active role seeding anisotropies in the CMB. (e.g. Pen *et al.* 1997). We will not discuss topological defects any further but we would like to point out that if such defects exist, they would produce anisotropies not only until the epoch of recombination but also at latter times. For instance, cosmic strings would generate in the temperature field a steplike discontinuity along the direction of the string, known as the *Kaiser-Stebbins* effect (Kaiser & Stebbins 1984).

In this section, we summarize the main sources that generate temperature anisotropies in the CMB (for a review see Hu *et al.* 1997) . The anisotropies are usually categorized according to their origin. Primary anisotropies are generated until the decoupling time, whereas secondary anisotropies are imprinted in the CMB during the way of the photons from the last scattering surface (LSS) to us.

Primary anisotropies in the CMB are comprised of three different contributions (e.g. Martínez-González *et al.* 1990). Then, if recombination occurs at the matter-dominated era and $\Omega \gtrsim 0.1$:

$$\frac{\Delta T}{T}(\vec{n}) \approx \frac{1}{4}\delta_{\gamma d} + \frac{1}{3}\phi_d - \vec{n}\vec{v_d} \tag{10}$$

where $\vec{n}$ is the direction given by the line of sight and the subscript d indicates quantities at decoupling time (using units with $c = 8\pi G \equiv 1$). The first term represents the anisotropy due to the photon density fluctuations at recombination (given approximately by equations (7) and (8) at decoupling for adiabatic and isocurvature perturbations, respectively). The gravitational redshift of photons climbing out of potential wells in their way from the LSS to us is given by the second term (known as Sachs-Wolfe effect). The third term represents the Doppler effect due to the peculiar velocities of the last scatterers of the photons.

The combination of these three terms, which are model-dependent, determines the main features of the angular power spectrum. The Sachs-Wolfe effect (Sachs & Wolfe 1967) dominates at scales larger than the horizon size at decoupling, $\theta \gtrsim 2^\circ\Omega^{1/2}$. At these scales, the initial perturbations can not be affected by causal processes and therefore, the CMB anisotropies (at $\ell \lesssim 20$) are directly related to the initial power spectrum of matter density fluctuations. If $P(k) \propto k^n$ then (Bond & Efstathiou 1987):

$$C_\ell^{SW} = Q_{\mathrm{rms-PS}}^2 \frac{4\pi}{5} \frac{\Gamma\left(\ell + \frac{n-1}{2}\right)\Gamma\left(\frac{9-n}{2}\right)}{\Gamma\left(\ell + \frac{5-n}{2}\right)\Gamma\left(\frac{3+n}{2}\right)}\,. \tag{11}$$

where $Q_{\mathrm{rms-PS}}^2$ is the quadrupole normalization. In particular, for a Harrison-Zel'dovich spectrum $C_\ell \propto 1/(\ell(\ell+1))$. This is reflected in the angular power spectrum (per logarithmic scale) as a *plateau* at low ℓ (see figure 1). These large scales are the ones probed by COBE. Several independent methods have been used to fit the quadrupole normalization and spectral index using the COBE data, which have leaded to consistent results with each other (Hinshaw *et al.* 1996, Górski 1994, Górski *et al.* 1996, Wright *et al.* 1996; see also Bennett *et al.* 1996 for a summary). For instance, Górski *et al.* (1996) obtain a quadrupole normalization $Q_{\mathrm{rms-PS}} = 15.3^{+3.7}_{-2.8}\mu K$ and a spectral index $n = 1.2 \pm 0.3$, which is compatible with a Harrison-Zel'dovich spectrum.

The anisotropies generated at intermediate angular scales ($0.1^\circ \lesssim \theta \lesssim 2^\circ$) are directly related to small-scale processes (inside the horizon) occurring until

decoupling time. In this way, acoustic oscillations of the baryon-photon fluid give rise to the so-called *Doppler peaks*. The position of these peaks is mainly determined by the geometry of the universe (e.g. Kamionkowski *et al.* 1994) due to the fact that the same physical scale subtends different angular scales depending on the curvature. For open universes, the angle is smaller and for closed universes is larger than in the flat case. Therefore, the Doppler peaks are shifted to smaller scales (larger ℓ's) for smaller values of Ω (as can be seen in figure 1).

At small scales, temperature fluctuations are damped due to the fact that decoupling is not instantaneous, i.e., the LSS has a finite thickness $\Delta z \sim 100$ (Jones & Wyse 1985). Thus, fluctuations with smaller scales than the thickness of the LSS will be reduced by averaging over photons coming from near and far parts of the LSS. This corresponds to scales $\theta \lesssim 10'\Omega^{1/2}$.

On the other hand, there are processes that decrease the matter and radiation density fluctuations at the LSS, therefore affecting the temperature anisotropies of the CMB. One of these mechanisms is the 'Silk damping' of adiabatic baryonic perturbations (Silk 1968). Photons diffuse out of overdense regions, 'dragging' the baryons with them. Therefore, a decrease in the density fluctuations of both baryons and radiation is produced. Silk damping only operates at small angular scales and does not affect any kind of present non-baryonic dark matter, since this matter is not coupled to radiation. However, there is a second process that can reduce the fluctuations of non-interacting, collisionless particles, such as the hypothetic constituents of dark matter (Bond & Szalay 1983). This mechanism is 'free streaming' of collisionless particles from high to low density regions. The damping of density fluctuations by this mechanism depends on the mass and velocity of the particles involved. Cold particles are not significantly affected by this process, since they move too slowly. On the other hand, the scale of density fluctuations affected by free streaming in the case of hot particles depends on their mass. For instance, for neutrinos with mass $m_\nu \sim 10eV$, density fluctuations can be strongly damped at scales corresponding to a supercluster of galaxies today (Bond & Szalay 1983).

6.2 Secondary anisotropies

Different processes occurring in the way of the photons from the LSS to the observer can generate secondary anisotropies in the CMB. Thus, they provide information about the evolution of the universe after decoupling. They can be categorized in gravitational and rescattering effects (for a more detailed description see Hu 1996, Hu *et al.* 1997).

6.2.1 Gravitational effects

Gravitation can induce secondary anisotropies in the CMB temperature field in different ways. One of such ways is the integrated Sachs-Wolfe (ISW) effect. When a photon falls in and climb out of a potential well, constant in time, the net change in the energy of the photon is zero. However, if the depth of the potential well varies as the photon crosses, the blueshift from falling in and the redshift from climbing out no longer cancel. The magnitude of the ISW is given by an integral along the photon's path (Martínez-González *et al.* 1990):

$$\frac{\Delta T}{T} = \int \frac{\partial \phi}{\partial t}(\vec{r}, t) dt \,. \tag{12}$$

On the other hand, gravity can also deflect the trajectory of a photon but without modifying its energy (gravitational lensing). The different cases that generate secondary anisotropies via these effects can be summarized as follows:

(i) In typical models, the epoch of matter-radiation equality occurs before recombination but not long before. Thus the photon contribution to the density of the universe is not completely negligible at last scattering and shortly thereafter. The decay in the potential shortly after last scattering gives rise to the *Early* ISW effect. This effect contributes at scales just larger than the first acoustic peak.

(ii) In open or Λ models, the potential decays at late times, typically at redshifts $z \lesssim \Omega^{-1}$. This produces the so-called *Late* ISW effect, that also shows up on large angular scales.

(iii) At late times, evolving non-linear structures cause the potential to vary with time. This kind of ISW effect is usually called the *Rees-Sciama* effect (Rees & Sciama 1968, Sanz *et al.* 1996). In standard CDM models, its contribution to the radiation power spectrum seems to be negligible except at very small angular scales. Thus, it is not likely to be detected by the next generation of satellites.

(iv) The ISW effect changes the energy of the photons but not their direction of motion. However, gravity can also produce the opposite effect via *gravitational lensing*: the trajectory of the photons is deflected but their energy is left unchanged. This effect slightly distorts the image of the LSS, producing a smearing of the angular power spectrum, with power from the peaks being moved into the valleys (Martínez-González *et al.* 1997). Although this effect is typically weak (a few percent change in the power spectrum), it could be detectable by some future CMB experiments.

(v) Other possible sources of secondary anisotropies are gravitational waves. The magnitude of the ISW effect is given in this case by an integral of the time derivative of the invariant metric perturbation along the photon's path (Sachs & Wolfe 1967). The gravitational waves would affect the radiation power spectrum at scales larger than the horizon at recombination

(Crittenden *et al.* 1994).

6.2.2 Scattering effects from reionization

Reionization of the universe after recombination produces free electrons that rescatter off the photons of the microwave background. Therefore, primary anisotropies are washed out and new secondary ones appear. If the universe becomes globally reionized at high redshift, primary anisotropies can be dramatically suppressed. On the other hand, local reionization also produces characteristic features in the CMB. For a recent review on reionization and its effects on the CMB see Haiman & Knox (1999).

(i) If the universe becomes globally reionized at a given redshift z_r, a certain fraction of the CMB photons will be rescattered by the free electrons. Therefore, a photon coming toward us from a particular direction, has not necessarily been originated from that direction. Thus, each location of the sky contains contributions from photons coming from different regions of the LSS, producing a damping of the fluctuations. The scales affected by this smearing are those smaller than the horizon size at the redshift z_r of the rescattering epoch. On the other hand, the fraction of CMB photons that are never rescattered is $e^{-\tau}$, where $\tau \equiv \sigma_T \int dt\, n_e$ (n_e is the electron density and σ_T is the Thomson cross-section) is the optical depth (see for instance Tegmark & Silk 1995).

(ii) Another source of secondary anisotropies in reionized universes is the so-called *Vishniac* effect (Ostriker & Vishniac 1986, Vishniac 1987). This is a second-order effect due to coupling between the bulk flow of the electrons and their density fluctuations that generates new anisotropies at very small angular scales.

(iii) Inverse Compton scattering of microwave photons by hot electrons in the intracluster gas of a cluster of galaxies produces spectral distortions in the blackbody spectrum of the CMB, known as the *thermal Sunyaev-Zel'dovich* (SZ) effect (Sunyaev & Zel'dovich 1970,1972). In addition, the peculiar velocities of clusters also produces secondary anisotropies in the CMB via the Doppler effect, known as the *kinetic SZ* effect (Sunyaev & Zel'dovich 1980). For a recent review on the SZ effect, see Birkinshaw 1999.

The thermal SZ has a characteristic frequency dependence. CMB photons that interact with electrons in the intracluster gas gain energy via inverse Compton scattering. This generates a decrease in the number of photons at frequencies lower than $\sim$ 217GHz and an increment at higher frequencies. The change of spectral intensity is given by:

$$\Delta I = \frac{2(kT_o)^3}{(hc)^2} \frac{x^4 e^x}{(e^x-1)^2} y \left[x coth\frac{x}{2} - 4 \right] \quad , \quad x = \frac{h\nu}{kT_o} \tag{13}$$

where $y \equiv \frac{k\sigma_T}{m_e} \int dl\ T_e n_e$ is the Comptonization parameter and is a function

of the electron density n_e and temperature T_e. This spectral dependence will help to separate the thermal SZ effect from the intrinsic cosmological signal in multifrequency observations.

On the other hand, the temperature fluctuation originated by the kinetic SZ effect is given by:

$$\frac{\Delta T}{T} = -\tau \frac{v_r}{c} \tag{14}$$

where v_r is the radial velocity of the cluster and τ is the optical depth.

The scales affected by these effects are those of the hot gas of cluster of galaxies, i.e., below a few arcmin. The amplitude of the thermal SZ effect is expected to be at the level of $\sim 10^{-6}$ at these scales whereas that of the kinetic SZ is ~ 10 times smaller. In addition, the kinetic SZ has the same spectral dependence that the CMB, because it is just a Doppler shift. This will make very difficult to separate this effect from the cosmological signal. On the other hand the angular power spectrum of the secondary anisotropies generated by the SZ effects is, approximately, that of a Gaussian noise, i.e., C_ℓ constant with ℓ.

Future space missions will observe a large number of clusters via the SZ effect. In particular, it is expected that the Planck mission will detect tens of thousands of clusters, although the exact number depends on the cosmological model (Aghanim *et al.* 1997). These data, combined with X-ray observations, will lead to an independent measurement of the Hubble constant (Cavaliere *et al.* 1977). In addition, all this information will provide an interesting tool to study different properties of the clusters, such as the cluster peculiar velocities (Haehnelt & Tegmark 1996).

(iv) It has been recently discussed that inhomogeneous reionization due to early formed stars or quasars could produce second order CMB fluctuations at subdegree scales through the Doppler effect (Aghanim *et al.* 1996, Gruzinov & Hu 1998, Knox *et al.* 1998, Peebles & Juszkiewicz 1998). However, calculations of their amplitudes are still highly uncertain and it is not clear whether they would significantly affect parameter estimation from the angular power spectrum of the CMB.

7 Foreground emissions

The microwave sky contains not only contribution from the CMB but also from several foreground components. In particular, the main foreground components are Galactic dust, free-free (bremsstrahlung) and synchrotron emission together with extragalactic point sources (for reviews see Davies 1999, Bouchet & Gispert 1999, Tegmark *et al.* 1999). In addition, a fourth Galactic foreground produced by spinning dust grains (Draine & Lazarian 1998) could

also be present, being detectable at frequencies $\sim 10 - 100$ GHz. In order to obtain all the valuable information contained on the CMB, it is necessary to separate the different contributions of the foregrounds from the cosmological signal. In addition, the foregrounds contain themselves very valuable information on astrophysical phenomena. Therefore, studying their contribution to the microwave sky becomes of great interest (see De Zotti 1999). In figure 2, the ranges of frequencies and multipoles where the different foregrounds dominate are shown for the 20% cleanest region of the sky. It can be seen that at low ℓ's Galactic contributions are more important, whereas point sources mainly affect at high ℓ's. On the other hand, the fluctuations produced by foreground emission present, in general, a non-Gaussian behaviour.

7.1 Synchrotron

Synchrotron emission is produced by relativistic electrons that are accelerated in magnetic fields (for reviews see Davies & Wilkinson 1998, Smoot 1999). Therefore, it depends on the energy spectrum of the electrons and on the intensity of the magnetic field (see Longair 1994). This component dominates the Galactic emission at low frequencies $\nu \lesssim 20$ GHz. The brightness temperature of synchrotron emission (or, equivalently, their intensity) is usually written in terms of a power law, $T_b \propto \nu^{-\beta_{\rm syn}}$. However, the synchrotron spectral index $\beta_{\rm syn}$ is expected to vary with frequency and position (Lawson *et al.* 1987).

The low frequency surveys by Haslam *et al.* (1982) at 408MHz (the only all-sky map available at these frequencies) and by Reich & Reich (1986) at 1420MHz have been normally used to estimate the amplitude of synchrotron emission at higher CMB frequencies by extrapolation. However, both of these maps are affected by significant uncertainties associated to the zero level, the gain stability and scanning errors. On the other hand, the spatial information is limited by their finite resolution, 0.85° and 0.6° for the Haslam and Reich & Reich maps, respectively.

For instance, a recent determination of $\beta_{\rm syn}$ in the range 1-10 GHz has been given by Platania *et al.* (1998). Combining the Haslam and Reich & Reich surveys with their own data obtained at the White Mountain, California (Smoot *et al.* 1985) with an angular resolution of 18°, they find a mean spectral index of $\beta_{\rm syn} = 2.76 \pm 0.11$ for a celestial region at declination 36°. Their data also suggest a steepening of the synchrotron spectrum toward higher frequencies. These results are consistent with previous estimations derived from different authors (see Platania *et al.* 1998 and references therein)

The angular power spectrum of the synchrotron emission is not well known.

It has been suggested that the Galactic power spectrum behaves as ℓ^{-3} as one approaches smaller angular scales (Tegmark & Efstathiou 1996). However, Lasenby (1997) has estimated the power spectrum of synchrotron for the high-latitude regions observed by the Tenerife experiment from the Haslam and Reich & Reich maps finding an angular power spectrum slightly flatter than the ℓ^{-3} law.

7.2 Free-free

The free-free emission is the thermal bremsstrahlung from hot ($T \gtrsim 10^4$K) electrons when accelerated by ions in the insterstellar gas (for reviews see Bartlett & Amram 1998, Smoot 1998). Free-free emission is the less well known Galactic foreground. This is due to the fact that it only dominates over a small range of frequencies ($\sim 25 - 75$ GHz), where the total Galactic emission is minimal. Therefore, it can not be traced by observing at higher or lower frequencies, unlike dust and synchrotron emission. However, diffuse Galactic H_α is thought to be a good tracer of free-free emission, since both are emitted by the same ionized medium (e.g. McCullough *et al.* 1999). The combination of WHAM (Haffner *et al.* 1998) observations with the southern celestial hemisphere H_α survey (McCullough *et al.* 1999) will allow to create in the near future a spatial template for free-free emission based on $H\alpha$ observations. At present, the only all-sky maps at frequencies of interest to study free-free are those of COBE. Bennett *et al.* (1992,1994) used a combination of the COBE DMR maps to get a free-free map at 53 GHz assuming a spectral index of $\beta_{\rm ff} = 2.15$ ($T_b \propto \nu^{-\beta_{\rm ff}}$). Using this technique, they found an amplitude for the free-free emission of $\Delta T = (10 \pm 4)\,\csc(|b|)\ \mu K$ for $|b| > 15^\circ$.

On the other hand, several authors (Kogut *et al.* 1996a, Leitch *et al.* 1997, de Oliveira-Costa *et al.* 1997) have found an anomalous component of Galactic emission at 15-40 GHz that correlates with the $100\mu m$ IRAS and DIRBE maps. Kogut *et al.* identifies this emission as a free-free component that correlates with the dust emission. However, it has been noted (e.g. Smoot 1998) that there are inconsistencies between the estimated level of free-free from $H\alpha$ and that implied from the correlation between free-free and dust emissions. A possible explanation for these inconsistencies is given by Draine & Lazarian (1998). They propose that emission from rotating dust grain could account, at least partially, for this anomalous component. This emission would be detectable at 10-100 GHz and would have a similar spectral dependence to free-free around $\nu = 25$ GHz. Recently, de Oliveira-Costa *et al.* (1999) have found the DIRBE-correlated Galactic emission of the Tenerife experiment to be better explained by dust rotating grains than by free-free emission. However, an independent analysis of the same data that is currently being performed does not favour either of the possibilities (Jones, private communication). Future

CMB experiments should be able to show what this anomalous component actually is.

Regarding the power spectrum of free-free emission, there are still uncertainties about its shape. Kogut *et al.* (1996a) found that the power spectrum of the dust-correlated free-free component was proportional to ℓ^{-3}. On the other hand, Veeraraghavan and Davies (1997) used H_α maps of the North Celestial Pole made by Gaustad *et al.* (1996) to estimate the free-free emission on scales of $10'$ to a few degrees. They found a best fit of $C_\ell^{\rm ff} \propto \ell^{-2.27\pm0.07}$, what it is significantly flatter than the ℓ^{-3} law. However, their normalization is also considerably lower than that derived from Kogut *et al.* resulting in a lower signal at all scales of interest.

7.3 Dust emission

Dust grains in our galaxy are heated by the interstellar radiation field, absorbing UV and optical photons and re-emitting the energy in the far infrared. The observed dust emission is the sum over the emission from each dust grain along the line of sight. This foreground dominates the Galactic emission at $\nu \gtrsim 90$ GHz.

Dust emission can be modelled by a modified blackbody emissivity law $I(\nu) \propto B_\nu(T_d)\nu^\alpha$ with $\alpha \simeq 2$ (Draine & Lee 1984). Wright *et al.* (1991) and Reach *et al.* (1995) found that two dust components were necessary to fit the Galactic dust emission, including a cold component with $T \sim 7K$. If this cold dust component exists, it could dominate the dust emission at low frequencies. However, the uncertainty about its existence is still very high. Kogut *et al.* (1996b) found that the high-latitude dust emission ($|b| > 20^\circ$) of the DMR-DIRBE maps is well fitted by a single dust component with temperature $T = 18^{+3}_{-7}$ and an emissivity index $\alpha = 1.9^{+3.0}_{-0.5}$.

Schlegel *et al.* (1998) combined the IRAS and DIRBE maps to construct an all-sky dust map at 100 μm with an angular resolution of $\sim 6'$. They also provided a map of dust temperature T_d by adopting a modified blackbody emissivity law with $\alpha = 2$. The dust temperature varies from 17 to $21K$. This map can be used as a dust template to extrapolate to the range of frequencies probed by future CMB experiments.

Gautier *et al.* (1992) estimated the dust power spectrum from the IRAS $100\mu m$ map, finding $C_\ell^{dust} \propto \ell^{-3}$ at scales $8^\circ - 4'$. This result has been confirmed by Wright (1998) using the DIRBE maps, who found $C_\ell \propto \ell^{-3}$ for $2 < \ell < 300$.

Emission from extragalactic point sources must be taken into account for the future high-resolution CMB experiments. Different source populations dominate above and below $\nu \sim 300$ GHz. At lower frequencies, radio sources give the main contribution whereas at higher frequencies, far-IR sources dominate. These populations mainly consist of compact AGN, blazars and radio loud QSOs in the radio and of inactive spirals galaxies in the far-IR. The number counts and spectral dependence of these populations are subject to many uncertainties due to the lack of surveys in the frequency range explored by CMB experiments. Detailed studies of the contribution of point sources at Planck frequencies have been performed by several authors (Toffolatti *et al.* 1998,1999, Bouchet & Gispert 1999, Guiderdoni 1999, Gawiser & Smoot 1997, Sokasian *et al.* 1998). According to the previous authors, it is expected that Planck will detect from several hundred to many thousand of sources as 5σ peaks at each frequency channel. Once the resolved point sources have been removed, we are left with a background due to the unresolved point sources. Following Bouchet & Gispert the confusion limit due to the Far Infrared sources background can be approximately treated as another template to be extracted from the data. Using the results of Guiderdoni *et al.* (1997,1998), the previous authors find the spectral behaviour of the infrared background to be approximately modelled as:

$$\ell C_\ell^{1/2} \simeq \frac{7.1\,10^{-9}}{e^{x/2.53}-1}\left(1-\frac{0.16}{x^4}\right)\frac{\sinh^2 x}{x^{0.3}}\ell\,[K]\,, \nu > 100\text{GHz},$$
$$\ell C_\ell^{1/2} \simeq 6.3\,10^{-9}\left(0.8-2.5x+3.38x^2\right)\frac{\sinh^2 x}{x^4}\ell\,[K]\,, \nu < 100\text{GHz}. \qquad (15)$$

where $x = h\nu/2kT_0 = \nu/(113.6\text{GHz})$. This estimation assumes that point sources have been removed by a simple thresholding technique at the 5σ level, but it is expected that their contribution can be subtracted down to lower fluxes. Thus the level of the unresolved point sources background given by eq.(15) can be seen as an upper limit to the contribution of the far IR population.

On the other hand, the previous expression does not take into account the population of point sources that dominate in low frequency and would therefore underestimate the contribution of point sources at the range of frequencies probed by the LFI and MAP. Assuming that point sources have been subtracted down to 100mJy, Toffolatti *et al.* obtain

$$\ell C_\ell^{1/2} \simeq \frac{\sinh^2\left(\frac{\nu}{113.6}\right)}{(\nu/1.5)^{(4.75-0.185\log(\nu/1.5))}}\ell\,[K] \qquad (16)$$

for the background due to the population dominating at low frequencies. The previous authors also predict that fluctuations from point sources will be well below the expected amplitude of the CMB fluctuations in the frequency range $50 - 200$GHz on all angular scales covered by the Planck Mission.

Regarding the power spectrum of point sources, this follows that of white noise, i.e., C_ℓ =constant for all scales, since point sources are, in a first approximation, randomly distributed in the sky. Thus, confusion from point sources mainly affects small angular scales (high ℓ's) as can be seen in figure 2. According to Toffolatti *et al.* , the fluctuations due to clustering are generally small in comparison with the Poissonian term but the relative importance of clustering increases if sources are subtracted down to faint flux limits.

8 Beyond the power spectrum

It has been already pointed out the importance of the angular power spectrum of the CMB, that completely describes the field in the case of Gaussian fluctuations as predicted by standard inflation. However, topological defects as well as certain inflationary models (e.g. Peebles 1999a,b) offer alternative scenarios of structure formation that give rise to non-Gaussianity in the CMB. Moreover, secondary anisotropies, such as the SZ effect, foreground contamination and systematics can well imprint a non-Gaussian signal in the CMB temperature fluctuations. Therefore, it becomes apparent the need of looking for non-Gaussianity in the CMB. Since the angular power spectrum only gives information about the 2-point correlation function, the use of statistics which introduce higher-order information from the random temperature field is necessary to test Gaussianity. In addition, these statistics can be used as a consistency check of the cosmological parameters determined from the angular power spectrum. Obtaining the set of C_ℓ's from future experiments, such as MAP or Planck, is not a trivial matter. Analysis of such complex and large data set presents a challenge for the existing and anticipated computers (for a discussion see Borrill 1999). Therefore, alternative statistics, computed from the data in a manner completely independent of the power spectrum, provide a useful check on the power spectrum computations, even in the case of underlying Gaussian fluctuations.

A large number of estimators to test non-Gaussianity in the CMB has been proposed. Most of them can be (semi)analytically calculated for Gaussian random fields, allowing a straightforward comparison of their expected value with the results computed from the data. Simulations are also extensively used to test the power of the different estimators. In this section we review some popular and novel estimators that have been suggested to test Gaussianity in the CMB:

(i) The simplest estimators are those directly related to the 1-point distribution function such as the *skewness* S_3 and *kurtosis* K_4 (Luo & Schramm 1993a) of the temperature fluctuations field:

$$S_3 = \frac{\mu_3}{\sigma^3} \quad , K_4 = \frac{\mu_4}{\sigma^4} - 3 \tag{17}$$

where σ, μ_3, μ_4 are the dispersion, third and fourth central moments of the distribution, respectively. Both quantities are zero for a Gaussian distribution.

Alternatively, the kurtosis of the gradient temperature map has also been considered by Moessner *et al.* (1994) to study the signal imprint by the Kaiser-Stebbins effect.

(ii) Another usual quantities to characterize non-Gaussianity are those based on the n-point correlation functions. In particular, the *3-point correlation function* (Luo & Schramm 1993b, Kogut *et al.* 1996c) is given by:

$$C_3(\theta_1, \theta_2, \theta_3) = \langle T(\mathbf{n_1}) T(\mathbf{n_2}) T(\mathbf{n_3}) \rangle \, , \tag{18}$$

where $\mathbf{n_1} \cdot \mathbf{n_2} = \cos\theta_1$, $\mathbf{n_2} \cdot \mathbf{n_3} = \cos\theta_2$ and $\mathbf{n_3} \cdot \mathbf{n_1} = \cos\theta_3$. Equivalently, the *bispectrum* can be used to test Gaussianity (Luo 1994, Heavens 1998, Ferreira *et al.* 1998, Spergel & Goldberg 1998a,b). This quantity plays the same role with respect to the 3-point correlation function than the angular power spectrum with respect to the 2-point correlation function. The bispectrum is defined as:

$$B(\ell_1 \ell_2 \ell_3, m_1, m_2, m_3) \equiv \langle a_{\ell_1 m 1} a_{\ell_2 m 2} a_{\ell_3 m 3} \rangle \tag{19}$$

Both, the 3-point correlation function and the bispectrum, are zero for a Gaussian distribution.

(iii) *Minkowski functionals* (Minkowski 1903) have also received extensive attention in the literature (Gott *et al.* 1990, Torres *et al.* 1995, Kogut *et al.* 1996c, Schmalzing & Górski 1997, Winitzki & Kosowsky 1997, Novikov *et al.* 1998). These quantities are local properties of the excursion sets above a threshold, translationally and rotationally invariant and additive. Therefore, they can be used for maps with incomplete or patchy sky coverage. For a 2-dimensional map, there are three Minkowski functionals: mean fractional area $< a >$ of excursion sets enclosed by the isotemperature contours, mean contour length $< s >$ per unit area and mean genus $< g >$ per unit area. The genus is a purely topological quantity that can be estimated as the total number of isolated high-temperature regions minus the number of holes in them. For a homogeneous and isotropic Gaussian field, the Minkowski functionals are given by

$$< a > = \frac{1}{2} \mathrm{erfc} \left(\frac{\nu}{\sqrt{2}} \right) \, ,$$

$$< s >= \frac{1}{2\theta_c} \exp^{-\nu^2/2} ,$$
$$< g >= \frac{1}{(2\pi)^{3/2}\theta_c^2} \nu \exp^{-\nu^2/2} , \quad (20)$$

where ν is a threshold defined in units of the field dispersion, erfc is the complementary error function and $\theta_c = (-C(0)/C''(0))^{1/2}$ is the coherence angle that depends only on the 2-point correlation function.

(iv) In addition to Minkowski functionals, several properties of excursions sets and maxima have been studied. They include the number and mean size (Sazhin 1985, Zabotin & Nasel'skii 1985, Bond & Efstathiou 1987, Vittorio & Juszkiewicz 1987, Martínez-González & Sanz 1989), eccentricity and Gaussian curvature (Barreiro *et al.* 1997, Martínez-González *et al.* 1999, Barreiro *et al.* 1999) and the probability density function of the hottest spot (Coles 1988). All the considered quantities can be (semi)analytically calculated for a Gaussian field. The mean area and number of excursion sets have also been calculated for some non-Gaussian fields derived from the Gaussian one (Coles & Barrow 1987). In particular the expected number of excursion sets $< N_s >$ over the whole sphere and their expected area $< A >$ for a homogeneous and isotropic Gaussian field can be estimated in the form (Vanmarcke 1983):

$$< N_s >= \frac{2}{\pi\theta_c^2} \frac{e^{-\nu^2}}{\mathrm{erfc}(\nu/\sqrt{2})} ,$$
$$< A >= \left(\pi\theta_c \exp(\nu^2/2)\mathrm{erfc}(\nu/\sqrt{2})\right)^2 . \quad (21)$$

Following the same direction, properties of clustering of maxima (Novikov & Jørgensen 1996), correlation of maxima (Bond & Efstathiou 1987, Kogut *et al.* 1995, Heavens & Sheth 1999) and correlation of excursion sets (Barreiro *et al.* 1998) have also been studied.

(v) Multifractal (Pompilio *et al.* 1995), partition function (Diego *et al.* 1999, Martínez-González *et al.* 1999) and roughness surface (Mollerach *et al.* 1999) based analysis are additional possibilities in the sought of non-Gaussianity. These methods provide an alternative way of studying the structure of CMB maps appearing at different scales.

(vi) So far, most of the described estimators are defined in real space. An interesting possibility is to use estimators based on Fourier statistics. A non-Gaussian signal can show up only in a particular scale, and the use of Fourier space allows to study each scale separately. On the contrary, spatial information is mixed up. An example of this kind of estimators is the so-called *non-Gaussian spectra* introduced by Ferreira & Magueijo (1997), which provides a way to characterize generic non-Gaussian fields. These quantities are extracted out of the angular distribution of the Fourier transform of the temperature anisotropies and take a simple form in the case of a Gaussian field. Another possibility is using a double Fourier transform, as

proposed by Lewin *et al.* (1999).

(vii) A promising novel possibility is the use of statistics based on wavelet techniques. Wavelets coefficients provide simultaneous information on the position and scale of the temperature field. Thus, they become a very useful tool to detect non-Gaussian signals that show up in a particular scale and in a given region of the sky. The wavelet coefficients of a Gaussian random field are also Gaussian distributed at each given scale. Thus, the skewness and kurtosis of those coefficients can be used to detect non-Gaussianity (Pando *et al.* 1998, Hobson *et al.* 1998b). Statistics based on higher order moments of temperature maps (or equivalently on cumulants) have been studied by Ferreira *et al.* (1997) defined in wavelet and Fourier spaces. Another possibility is the study of the scale-scale correlation of the temperature field through wavelet coefficients (Pando *et al.* 1998).

The power of a given estimator in detecting non-Gaussianity will strongly depend on the considered non-Gaussian field. A particular estimator can perform very well in detecting some kind of non-Gaussian signal and fail to detect a different one. They have been usually applied to different cases and a comparative study becomes necessary before general conclusions can be established. A detailed description of the different tests performed for each of the proposed non-Gaussian estimators is out of the scope of this review. However, we will refer here to the tests of Gaussianity that have been applied to the COBE data. Their different performance can give us some hints about the power of the corresponding method. Torres (1994) used the number of hot spots and their genus to study the 1-yr COBE data. He found the data to be consistent with being derived from a parent Gaussian distribution. Kogut *et al.* (1995,1996c) tested their Gaussianity through the genus, the 3-point correlation function and the extrema correlation. The result is again that the data are compatible with a Gaussian distribution. Moreover, comparison with non-Gaussian toy models show the Gaussian distribution to be the most probable one of all the considered cases. They also find the extrema correlation to be a better discriminator than the genus and 3-point correlation function. Schmalzing & Gorski (1997), Heavens (1998) and Diego *et al.* (1999) also found the COBE data to be consistent with a Gaussian field using the Minkowski functionals, the bispectrum and a partition function analysis, respectively. However, detection of non-Gaussianity in the COBE data has been reported by two groups, although the origin of this non-Gaussian signal may well not be cosmological. Ferreira *et al.* (1998) studied the distribution of an estimator for the normalized bispectrum, finding that Gaussianity is ruled out at the confidence level $> 98\%$. However, Banday *et al.* (1999) showed in a recent work that the non-Gaussian signal detected by Ferreira *et al.* (1998) is likely due to a systematic effect. On the other hand, Pando *et al.* (1998) performed a discrete wavelet analysis based on scale-scale correlation and find a significant non-Gaussian signal that rules out Gaussianity at the 99% level, although the same authors do not find significant deviation from Gaussianity using the skewness

and kurtosis of wavelet coefficients at each scale. However, the same analysis has been independently performed by Mukherjee *et al.* (1999), who are unable to reproduce the numerical results obtained by Pando *et al.* and do not find strong evidence for non-Gaussianity in the scales probed by COBE. The previous authors conclude that wavelet analysis only rule out Gaussinity at the 76% level. For a discussion of the statistical significance of these detections of non-Gaussianity see Bromley & Tegmark (1999).

Finally we would like to go back to the use of alternative estimators as an independent consistency check of the computed results from the power spectrum. Several authors have used alternative estimators to the 2-point correlation function to fit the amplitude and spectral index of the power spectrum of the COBE data. In this direction, Torres *et al.* (1995) performed an analysis based on the genus and number of spots, Diego *et al.* (1999) used a partition function technique and Mollerach *et al.* (1999) studied the roughness of the temperature surface. All these works report consistent results with the ones found by more standard methods. Park *et al.* (1998) studied the 2-point correlation function and genus of Gaussian simulations of MAP data. They found the genus to be a good independent test of the cosmological parameters computed from the power spectrum. Barreiro *et al.* (1997) pointed out the interest of studying topological quantities of CMB maps to discriminate between different Ω values and Wandelt *et al.* (1998) developed tools for their study on high-resolution CMB simulations.

9 Image reconstruction methods

Future CMB data will provide an extremely valuable information. However, these maps will contain not only the cosmological signal but also the contribution from the different foregrounds (see § 7) together with instrumental noise. Therefore, before extracting all the information coded in the CMB, 'cleaning' of the maps and a separation of the microwave sky components must be performed.

Many methods have been proposed in Astronomy and other fields to reconstruct a signal from noisy data. In the present section we will outline the basis of three of these methods as applied to a general image and comment on their performance when applied to CMB simulations. For a comparison of different methods as applied to CMB, see Tegmark (1997) and Jones (1998).

9.1 Wiener Filter

Consider a set of N measured data $\mathbf{d} = (d_1, d_2, ..., d_N)$ that we use to estimate the underlying signal or image $\mathbf{s} = (s_1, s_2, ..., s_M)$. We will consider the case in which the data vector $\mathbf{d}$ can be written as a linear convolution of the signal:

$$\mathbf{d} = \mathbf{R}\mathbf{s} + \mathbf{n}\,, \tag{22}$$

where $\mathbf{R}$ is some known $N \times M$ matrix and $\mathbf{n}$ is a random noise vector. $\mathbf{R}$ usually represents the antenna response of the instrument to the underlying field, although it can also include a more complicated relationship between the measured data and the signal.

In order to apply Wiener Filter, some assumptions are usually made. The noise and signal are taken to have zero mean and we assume knowledge of the covariance matrices:

$$\begin{aligned} \mathbf{S} &= < \mathbf{s}\mathbf{s}^t >\,, \\ \mathbf{N} &= < \mathbf{n}\mathbf{n}^t > \ . \end{aligned} \tag{23}$$

In addition, signal and noise are taken to be uncorrelated:

$$< \mathbf{n}\mathbf{s}^t >= 0\,. \tag{24}$$

Given an estimator of the signal $\hat{\mathbf{s}}$, the reconstruction error is given by:

$$\boldsymbol{\epsilon} = \mathbf{s} - \hat{\mathbf{s}}\,. \tag{25}$$

Wiener filter (Wiener 1949) is defined as the linear filter $\mathbf{W}$, i.e. $\hat{\mathbf{s}} = \mathbf{W}\mathbf{d}$, that minimises the variance of the reconstruction error $< |\boldsymbol{\epsilon}|^2 >$. Carrying out the minimisation, $\mathbf{W}$ is found to be (e.g. Rybicki & Press 1992) :

$$\mathbf{W} = \mathbf{S}\mathbf{R}^t \left(\mathbf{R}\mathbf{S}\mathbf{R}^t + \mathbf{N}\right)^{-1}\ . \tag{26}$$

If the signal and noise are Gaussian random variables, this filter can also be obtained as the Bayesian estimator of the signal (e.g. Bunn *et al.* 1996). Derivations of Wiener filter in Fourier and harmonic space can be found for instance in Press *et al.* (1994) and Bunn *et al.* (1996), respectively. Wiener filter has been applied to the reconstruction of CMB maps from different experiments, such as COBE (Bunn *et al.* 1994,1996) and Saskatoon (Tegmark *et al.* 1997). The bottom panels of figure 3 reproduces an example of the performance of Wiener filter for a CMB simulation of a standard flat CDM

Fig. 3. Simulated map of the cosmological signal for a standard CDM model (top left), signal plus Gaussian noise with $S/N = 1$ (top right), denoised map using wavelets (middle left), residual map obtained from the CMB signal map minus the denoised one (middle right), denoised map using Wiener filter (bottom left) and the corresponding residuals (bottom right).

model plus Gaussian noise with a signal to noise ratio $S/N = 1$. The level of noise is greatly reduced (by a factor ~ 5) in the reconstructed image, although the small scale structure of the signal is also suppressed.

Methods based on Wiener filter are one of the alternatives to reconstruct the cosmological signal as well as the foregrounds from the future multifrequency all-sky CMB data (Tegmark & Efstathiou 1996).

9.2 Maximum Entropy Method

The maximum entropy method (MEM) is derived in the context of the Bayesian formalism. Bayes' theorem states that the posterior probability $P(\mathbf{s}|\mathbf{d})$ of an underlying signal $\mathbf{s}$ given some data $\mathbf{d}$ is proportional to:

$$P(\mathbf{s}|\mathbf{d}) \propto P(\mathbf{d}|\mathbf{s})P(\mathbf{s})\,, \tag{27}$$

where $P(\mathbf{d}|\mathbf{s})$ is the likelihood (probability of obtaining a set of data given an underlying signal) and $P(\mathbf{s})$ is the prior probability. The Bayesian estimator $\hat{\mathbf{s}}$ of the signal is chosen to be the one that maximises the posterior probability given in equation(27). The form of the likelihood is determined from the data. For the case of Gaussian noise (assumed to have zero mean for simplicity), the likelihood is a N-multivariate Gaussian distribution:

$$P(\mathbf{d}|\mathbf{s}) \propto \exp\left[-\frac{1}{2}(\mathbf{d}-\mathbf{R}\mathbf{s})^t\mathbf{N}^{-1}(\mathbf{d}-\mathbf{R}\mathbf{s})\right] \propto \exp\left(-\frac{\chi^2}{2}\right)\,. \tag{28}$$

On the other hand, we must assume a prior probability, which includes our knowledge from the underlying signal. A possible choice is given by MEM. This method introduces a conservative prior, that chooses, from all the possible signals compatible with the data, the one with less structure. The entropic prior is given by (Skilling 1989):

$$P(\mathbf{s}) \propto \exp\left[\alpha S(\mathbf{s},\mathbf{m})\right]\,, \tag{29}$$

where $\mathbf{m}$ is a model vector to which $\mathbf{s}$ defaults in the absence of data and α is a constant that depends on the scaling of the problem. The function $S(\mathbf{s},\mathbf{m})$ is the cross entropy of $\mathbf{s}$ and $\mathbf{m}$. For the case of a positive additive distribution,

as is the case in standard applications of maximum entropy, $S(\mathbf{s}, \mathbf{m})$ is given by (Skilling 1989):

$$S(\mathbf{s}, \mathbf{m}) = \sum_{i=1}^{M} \left(s_i - m_i - s_i ln \left[\frac{s_i}{m_i} \right] \right) . \tag{30}$$

However, in the case of the CMB, there are both positive and negative fluctuations. Therefore, this expression needs to be generalized for images that take positive and negative values. This is done by considering the image to be the difference of two positive additive distributions $\mathbf{s} = \mathbf{u} - \mathbf{v}$ (Hobson & Lasenby 1998), obtaining for $S(\mathbf{s}, \mathbf{m})$:

$$S(\mathbf{s}, \mathbf{m}) = \sum_{i=1}^{M} \left(\psi_i - m_{ui} - m_{vi} - s_i \ln \left[\frac{\psi_i + s_i}{2m_{ui}} \right] \right) , \tag{31}$$

where $\psi_i = (s_i^2 + 4m_{ui}m_{vi})^{1/2}$ and $\mathbf{m}_u$ and $\mathbf{m}_v$ are separated models for $\mathbf{u}$ and $\mathbf{v}$, respectively.

Thus, the posterior probability can be written as:

$$P(\mathbf{s}|\mathbf{d}) \propto \exp \left(-\frac{\chi^2}{2} + \alpha S(\mathbf{s}, \mathbf{m}) \right) . \tag{32}$$

Therefore, maximising $P(\mathbf{s}|\mathbf{d})$ is equivalent to minimise the quantity $\phi = \frac{\chi^2}{2} - \alpha S$. The constant α can be interpreted as a regularising parameter of the relative weight of the data and the prior. One possible way to determine α is introducing it as an extra parameter in the Bayesian framework (see Skilling 1989, Hobson *et al.* 1998a).

Different choices of the prior are possible, resulting in different reconstructions. In particular, for the case of a Gaussian prior, we recover the Wiener filter. Actually, MEM and Wiener filter are closely related. It can be shown, that in the small fluctuation limit, Wiener filter can be recovered as a quadratic approximation to MEM (e.g. Hobson *et al.* 1998a). For a comparison of the performance of both methods see Hobson *et al.* 1998a.

MEM has been applied to CMB data obtained from different experiments (White & Bunn 1995, Jones 1998, Jones *et al.* 1998) as well as to simulations of the future satellite missions (Hobson *et al.* 1998a,1999, Jones *et al.* 1999). In particular, a Fourier-space MEM has been used by the previous authors to perform a separation of the different components of the microwave sky for Planck simulations of size $10^\circ \times 10^\circ$. In addition to the cosmological signal and the instrumental noise, the simulations include the contribution of the Galactic components (dust, free-free and synchrotron), extragalactic point sources

as well as the thermal and kinetic SZ effects from cluster of galaxies. The method performs very well, producing accurate maps and power spectra of the CMB. Moreover, given some prior knowledge of the power spectra of the CMB and foregrounds, it is also possible to recover accurate reconstructions of the thermal SZ effect and the Galactic components. In addition, precise catalogues of point sources can be recovered at each of the Planck frequency channels.

9.3 Wavelet techniques

The development of wavelet techniques applied to signal processing has been very fast in the last ten years. They are known to be very efficient in dealing with problems of data compression and denoising and could be a good alternative to analyse CMB data. The property that makes wavelets so interesting is that they keep a good space-frequency localization. Each point of the signal is associated to a set of wavelet coefficients corresponding to different scales. Thus, unlike the Fourier transform, the wavelet transform allows to have information about the importance of different scales at each position. There is not a unique choice for the wavelet basis. We will only consider here the 1-dimensional case for discrete, orthogonal and compactly-supported wavelet bases. The basis is constructed from dilations and translations of the *mother* (or *analysing*) wavelet function ψ and a second related function $\phi(x)$ called the *father* (or *scaling*) function:

$$\begin{aligned}\psi_{j,l} &= 2^{\frac{j-n}{2}}\psi\left(2^{j-n}x-l\right)\,,\\ \phi_{j,l} &= 2^{\frac{j-n}{2}}\phi\left(2^{j-n}x-l\right)\,,\end{aligned} \tag{33}$$

where $0 \geq j \geq n-1$ and $0 \geq l \geq 2^j-1$ are integer denoting the dilation and translation indices, respectively, and 2^n is the number of pixels of the considered discrete signal $f(x)$. ψ and ϕ must together satisfy some mathematical relations, as first shown by Daubechies (1988). In particular, the most straightforward requirements are:

$$\begin{aligned}&\int \psi(x)dx = 0\,,\\ &\int \phi(x)dx = 1\,.\end{aligned} \tag{34}$$

The reconstruction of the signal $f(x)$ using the wavelet basis is given by:

$$f(x) = a_{0,0}\phi_{0,0}(x) + \sum_j \sum_l w_{j,l}\psi_{j,l}(x)\,, \tag{35}$$

being a, w the wavelet coefficients defined as:

$$a_{0,0} = \int f(x)\phi_{0,0}(x)dx\,,$$
$$w_{j,l} = \int f(x)\psi_{j,l}(x)dx\,. \tag{36}$$

Denoising of data using wavelets are based on the different scale properties of noise and signal. The idea is to keep those coefficients dominated by the signal and set to zero those where the noise is the main contribution. This can be achieved by using thresholding techniques. Given a set of data $\mathbf{d}$, we can recover the underlying signal by acting over the data wavelet coefficients $w_{j,l}$ in the following way:

$$\hat{w}_{j,l} = \begin{cases} w_{j,l} - \nu\sigma_n \text{ if } w_{j,l} > \nu\sigma_n \\ 0 \qquad\qquad \text{if } |w_{j,l}| \leq \nu\sigma_n \\ w_{j,l} + \nu\sigma_n \text{ if } w_{j,l} < -\nu\sigma_n \end{cases} \tag{37}$$

This is known as a *soft* threshold (Donoho & Jonhstone 1995). ν is the threshold defined in units of the dispersion of the noise σ_n at each scale. For the case of orthogonal wavelets and uncorrelated noise, σ_n is constant over all the different scales. By inverse transforming the thresholded coefficients we get an estimation of the underlying signal, where the noise has been highly suppressed. The choice of the threshold can be made using signal-independent prescriptions such as the Stein's Unbiased Risk Estimate (SURE) (e.g. Ogden 1997).

Wavelet techniques have been applied to very different fields in the last years. However, only very recently some works have studied their performance when dealing with CMB maps (Sanz *et al.* 1999a,b, Tenorio *et al.* 1999). The middle panels of Figure 3 show the reconstructed image obtained by applying a wavelet thresholding technique, as discussed by Sanz *et al.* 1999b. Even although knowledge of the power spectrum of the original signal is not required for this technique, the noise is suppressed as efficiently as in the Wiener filter case. In addition, the power spectrum is recovered up to $\ell \lesssim 1700$ for $S/N \leq 1$ with an error $\lesssim 20\%$ what is considerably better than the power spectrum of the reconstructed image provided by Wiener filter. However, the non-linearity of the soft thresholding technique is introducing a certain level of non-Gaussianity, what must be taken into account when analysing the data. This application considers only the presence of the cosmological signal plus Gaussian noise, being just a first approach that pretends to shed light on the wavelet characterization of the different components. The final goal would be a Bayesian framework (incorporating entropy or other constraints) dealing

with wavelet components at different scales and introducing multifrequency information. Following this direction, some work has already been carried out by Jewell *et al.* 1999.

In addition to denoising, wavelet techniques are good in detecting structure. For instance, the mexican hat wavelet (a non-orthogonal wavelet) seems to be a good tool to detect and subtract point sources from the CMB (Cayón *et al.* 1999).

10 Conclusions

In this paper, we have reviewed the present status of CMB experiments, summarize some basics aspects of the theory, describe some relevant characteristics of the foregrounds, review the methods proposed to test Gaussianity and outline the reconstruction methods recently applied to CMB.

During the last years there has been an explosion of experiments dedicated to measuring the CMB anisotropies, including balloon-borne and ground based instruments. More than a dozen groups have reported the detection of CMB anisotropies. In addition two satellite missions, MAP and Planck, will provide with multifrequency all-sky CMB data with unprecedented resolution and sensitivity. In order to obtain all the valuable information encoded in the CMB, a good understanding of the underlying theory is necessary and we have reviewed the basics of primary and secondary anisotropies. On the other hand, our ability to measure the cosmological parameters will also depend on the removal of the Galactic and extragalactic foregrounds. We have reviewed the current knowledge of these contaminants, pointing out the presence of an anomalous component. Further study of these foregrounds becomes necessary in order to analyse successfully the CMB data. One of the key issues expected to be solved with the future CMB data is whether the temperature anisotropy field is Gaussian as predicted by the standard inflationary model. Numerous tests have been proposed to detect non-Gaussianity in the CMB, some of them looking very promising. However, before any general conclusion can be established, a direct comparison of the different methods is necessary. These tests, computed from the data in a manner completely independent of the $C_\ell's$, also provide a useful check on the conclusions derived from the power spectrum, even in the case of underlying Gaussian fluctuations. Finally, we have briefly described the basics of reconstruction methods recently applied to the CMB, including Wiener filter, the maximum entropy method and wavelet techniques. The development of an integrated scheme combining the power of Bayesian methods and the excellent properties of wavelet techniques is one of the promising projects left for the future in order to separate and reconstruct the different components of the microwave sky.

Acknowledgement

RBB thanks José Luis Sanz and Enrique Martínez-González for a careful reading of the manuscript, Laura Cayón and Patricio Vielva for useful comments and Max Tegmark for kindly providing one of the figures. This work has been supported by the DGESIC Project no. PB95-1132-C02-02, CICYT Acción Especial no. ESP98-1545-E and Comisión Conjunta Hispano-Norteamericana de Cooperación Científica y Tecnológica with ref. 98138. The author also acknowledges financial support from a Spanish MEC fellowship and from the PPARC in the form of a research grant.

References

[1] Aghanim N., De Luca A., Bouchet F.R., Gispert G. & Puget J.L., 1997, A&A, 325, 9

[2] Aghanim N., Désert F.X., Puget J.L. & Gispert R., 1996, A&A, 311,1; see also erratum to appear in A&A, preprint astro-ph/9811054

[3] Albrecth A. & Steinhardt P.J., 1982, Phys.Rev.Lett., 48, 1220

[4] Alpher R.A. & Herman R.C., 1948, Nature, 162, 774

[5] Avelino P.P., Caldwell R.R. & Martins C.J.A.P., 1998, preprint astro-ph/9809130

[6] Baker J.C. *et al.* , 1999, preprint astro-ph/9904415

[7] Banday A.J., Zaroubi S. & Górski K.M., 1999, submitted to ApJ, preprint astro-ph/9908070

[8] Bardeen J.M., Steinhardt P.J. & Turner M.S., 1983, Phys.Rev., D28, 679

[9] Barreiro R.B., Sanz J.L., Martínez-González E., Cayón L. & Silk J., 1997, ApJ, 478, 1

[10] Barreiro R.B., Sanz J.L., Martínez-González E., & Silk J., 1998, MNRAS, 296, 693

[11] Barreiro R.B. *et al.* , 1999, in preparation

[12] Bartlett J.G. & Amram P., 1998, in 'Fundamental parameters in cosmology', Proc. of the XXXIIIrd rencontres de Moriond (France), Trân Thanh Vân J., Giraoud-Héraud Y., Bouchet F., Damour T. & Mellier Y. eds., Editions Frontiéres, p.183

[13] Bennett C.L. *et al.* , 1992, ApJ, 396, L7

[14] Bennett C.L. *et al.* , 1994, ApJ, 436, 423

[15] Bennett C.L. *et al.* , 1996, ApJ, 464, L1

[16] Birkinshaw M., 1999, Phys.Rept., 310, 97

[17] Bond J.R., 1995, Astrophys. Lett. Comm., 32, 63

[18] Bond J.R. & Efstathiou G., 1987, MNRAS, 226, 655

[19] Bond J.R., Efstathiou G. & Tegmark M., 1997, MNRAS, 291, L33

[20] Bond J.R. & Szalay A.S., 1983, ApJ, 274, 443

[21] Borrill J., 1999, Phys.Rev.D, in press, preprint astro-ph/9712121

[22] Bouchet F.R. & Gispert R., 1999, submitted to New Astronomy, preprint astro-ph/9903176

[23] Bromley B.C. & Tegmark M., 1999, preprint astro-ph/9904254

[24] Bunn E.F., Fisher K.B., Hoffman Y., Lahav O., Silk J. & Zaroubi S., 1994, ApJ, 432, L75

[25] Bunn E.F., Hoffman Y. & Silk J., 1996, ApJ, 464, 1

[26] Cavaliere A., Danese L. & De Zotti G., 1977, ApJ, 217, 6

[27] Cayón L., 1996, in 'The Universe at high z, large scale structure and the cosmic microwave background', Proc. of the advanced summer school held at Laredo (Spain), Martínez-González E. & Sanz J.L. eds., Springer-Verlag, p.177

[28] Cayón L., Sanz J.L., Barreiro R.B., Martínez-González E., Vielva P., Toffolatti L., Silk J., Diego J.M. & Argüeso F., 1999, submitted to MNRAS

[29] Coble K. *et al.* , 1999, preprint astro-ph/9902195

[30] Coles P., 1988, MNRAS, 231, 125

[31] Coles P. & Barrow J.D., 1987, MNRAS, 228, 407

[32] Crittenden R., Bond J.R., Davis R.L., Efstathiou G. & Steinhardt P.J., 1994, Phys.Rev.Lett., 71, 324

[33] Daubechies I., 1988, Comm. Pure Appl. Math., 41, 909

[34] Davies R.D. 1999, Astrophys. Lett. Comm., in press

[35] Davies R.D. & Wilkinson A., 1998, in 'Fundamental parameters in cosmology', Proc. of the XXXIIIrd rencontres de Moriond (France), Trân Thanh Vân J., Giraoud-Héraud Y., Bouchet F., Damour T. & Mellier Y. eds., Editions Frontiéres, p.175

[36] de Bernardis P. *et al.* , 1994, ApJ, 422, L33

[37] de Bernardis P. & Masi S., 1998, in 'Fundamental parameters in cosmology', Proc. of the XXXIIIrd rencontres de Moriond (France), Trân Thanh Vân J., Giraoud-Héraud Y., Bouchet F., Damour T. & Mellier Y. eds., Editions Frontiéres, p.209

[38] de Oliveira-Costa A., Devlin M.J., Herbig T., Miller A. D., Netterfield C.B., Page L.A. & Tegmark M., 1998, ApJ, 509, L77

[39] de Oliveira-Costa A., Kogut A., Devlin M.J., Netterfield C.B., Page L.A. & Wollack E.J., 1997, ApJ, 482, L17

[40] de Oliveira-Costa A., Tegmark M., Gutiérrez C.M., Jones A.W., Davies R.D., Lasenby A.N., Rebolo R. & Watson R.A., 1999, submitted to ApJL, preprint astro-ph/9904296

[41] De Zotti G., Toffolatti L., Argüeso F., Davies R.D., Mazzotta P., Partridge R.B., Smoot G.F. & Vittorio N., 1999, Proc. of the Conference '3K Cosmology' held in Italy, in press, preprint astsro-ph/9902103

[42] Dicker S.R., Melhuish S.J., Davies R.D., Gutiérrez C.M., Rebolo R., Harrison D.L., Davis R.J., Wilkinson A., Hoyland R.J. & Watson R.A., 1999, MNRAS, in presss, preprint astro-ph/9907118

[43] Diego J.M., Martínez-González E., Sanz J.L., Mollerach S. & Martínez V.J., 1999, MNRAS, in press, preprint astro-ph/9902134

[44] Donoho D.L. & Johnstone I.M., 1995, Journal of the American Statistical Association, 90, 1200

[45] Draine B.T. & Lazarian A., 1998, ApJ, 494, L19

[46] Draine B.T. & Lee H.M., 1984, ApJ, 285, 89

[47] Efstathiou G. & Bond J.R., 1986, MNRAS, 218, 103

[48] Femenia B., Rebolo R., Gutiérrez C.M., Limon M. & Piccirillo L., 1998, ApJ, 498, 117

[49] Ferreira P.G. & Magueijo J., 1997, Phys.Rev., D55, 3358

[50] Ferreira P.G., Magueijo J. & Górski K.M., 1998, ApJ, 503, L1

[51] Ferreira P.G., Magueijo J. & Silk J., 1997, Phys.Rev., D56, 4592

[52] Fixsen D.J., Cheng J.M., Gales J.C., Mather J.C., Shafer R.A. & Wright E.L., 1996, ApJ, 473, 576

[53] Gamow, G. 1948a, Phys.Rev., 74, 505

[54] Gamow, G. 1948b, Nature, 162, 680

[55] Ganga K., Page L., Cheng E.S. & Meyer S., 1994, ApJ, 432, L15

[56] Gaustad J., McCullough P. & van Buren D., 1996, P.A.S.P., 108, 351

[57] Gautier T.N.I., Boulanger F., Perault M. & Puget J.L., 1992, Astron.J., 103, 1313

[58] Gawiser E. & Smoot G.F., 1997, ApJ, 480, L1

[59] Górski K.M., 1994, ApJ, 430, L85

[60] Górski K.M., Banday A.J., Bennett C.L., Hinshaw G., Kogut A., Smoot G.F. & Wright E.L., 1996, ApJ, 464, L11

[61] Gott III J.R., Park C., Juszkiewicz R., Bies W.E., Bennett D.P., Bouchet F.R. & Stebbins A., 1990, ApJ, 352, 1

[62] Griffiths L.M., Barbosa D. & Liddle A.R., 1998, preprint astro-ph/9812125

[63] Gruzinov A. & Hu W., 1998, ApJ, 508, 435

[64] Guiderdoni B., 1999, in 'Microwave Foregrounds', ASP Conference Series, Vol.181, A.de Oliveira-Costa and M.Tegmark eds., p.173

[65] Guiderdoni B., Bouchet F.R., Puget J.L., Lagache G. & Hivon E., 1997, Nature, 390, 257

[66] Guiderdoni B., Hivon E., Bouchet F.R. & Maffei B., 1998, MNRAS, 295, 877

[67] Gundersen J.O. *et al.* , 1995, ApJ, 443, L57

[68] Guth A.H., 1982, Phil. Trans. R. Soc., A307, 141

[69] Guth A.H. & Pi S.Y., 1982, Phys.Rev.Lett., 49,1110

[70] Gutiérrez C., Rebolo R., Watson R.A., Davies R.D., Jones A.W. & Lasenby A.N., 1999, preprint astro-ph/9903196

[71] Haehnelt M. & Tegmark M., 1996, MNRAS, 279, 545

[72] Haffner L.M., Reynolds R.J. & Tufte S.L., 1998, ApJ, 501, L83

[73] Haiman Z. & Knox L., 1999, in 'Microwave Foregrounds', ASP Conference Series, Vol.181, A.de Oliveira-Costa and M.Tegmark eds., p.227

[74] Halpern M. & Scott D., 1999, in 'Microwave Foregrounds', ASP Conference Series, Vol.181, A.de Oliveira-Costa and M.Tegmark eds., p.283

[75] Harrison E.R., 1970, Phys.Rev., D1, 2726

[76] Haslam C.G.T., Klein U., Salter C.J., Stoffel H., Wilson W.E., Cleary M.N., Cooke D.J. & Thomasson P., 1982, Astr. Ap., 100, 209

[77] Hawking S.W., 1982, Phys.Lett., 115B, 295

[78] Heavens A.F., 1998, MNRAS, 299, 805

[79] Heavens A.F. & Sheth R.K., 1999, MNRAS, in press, preprint astro-ph/9904307

[80] Hinshaw G., Banday A.J., Bennett C.L., Górski K.M., Kogut A., Smoot G.F. & Wright E.L., 1996, ApJ, 464, L17

[81] Hobson M.P., Barreiro R.B., Toffolatti L., Lasenby A.N., Sanz J.L., Jones A.W. & Bouchet F.R., 1999, MNRAS, 306, 232

[82] Hobson M.P., Jones A.W., Lasenby A.N. & Bouchet F., 1998a, MNRAS, 300, 1

[83] Hobson M.P., Jones A.W. & Lasenby A.N., 1998b, preprint astro-ph/9810200

[84] Hobson M.P. & Lasenby A.N., 1998, MNRAS, 298, 905

[85] Hu W., 1996, in 'The Universe at high z, large scale structure and the cosmic microwave background', Proc. of the advanced summer school held at Laredo (Spain), Martínez-González E. & Sanz J.L. eds., Springer-Verlag, p.207

[86] Hu W., Seljak U., White M. & Zaldarriaga M. 1998, Phys.Rev., D57, 3290

[87] Hu W., Sugiyama N. & Silk J., 1997, Nature, 386, 37

[88] Jeannerot R., 1996, Phys.Rev., D53, 5426

[89] Jewell J., Lawrence C.R. & Levin S., 1999, in 'Microwave Foregrounds', ASP Conference Series, Vol.181, A.de Oliveira-Costa and M.Tegmark eds., p.357

[90] Jones A.W., 1998, 'Application of novel analysis techniques to Cosmic Microwave Background Astronomy', PhD thesis, U.Cambridge

[91] Jones A.W., Hancock S., Lasenby A.N., Davies R.D., Gutiérrez C.M., Rocha G., Watson R.A. & Rebolo R., 1998, MNRAS, 294, 582

[92] Jones A.W., Hobson M.P. & Lasenby A.N., 1999, MNRAS, 305, 898

[93] Jones B.J.T. & Wyse R.F.G., 1985, A&A, 149, 144

[94] Kaiser N. & Stebbins A., 1984, Nature, 310, 391

[95] Kamionkowski M., Spergel D.N. & Sugiyama N., 1994, ApJ, 426, 57

[96] Knox L., Scoccimarro R. & Dodelson S., 1998, Phys.Rev.Lett., 81, 2004

[97] Kogut A., Banday A.J., Bennett C.L., Hinshaw G., Lubin P.M. & Smoot G.F., 1995, ApJL, 439, L29

[98] Kogut A., Banday A.J., Bennett C.L., Górski K., Hinshaw G., Smoot G.F. & Wright E.L., 1996a, ApJ, 464, L5

[99] Kogut A., Banday A.J., Bennett C.L., Górski K., Hinshaw G., Reach W.T., 1996b, ApJ, 460, 1

[100] Kogut A., Banday A.J., Bennett C.L., Górski K., Hinshaw G., Smoot G.F. & Wright E.L., 1996c, ApJ, 464, L29

[101] Kolb E.B. & Turner M., 1990,'The Early Universe', Addison-Wesley, New York

[102] Lasenby A.N., 1997, in 'Microwave Background Anisotropies', Proc. XVIth Moriond Astrophysics Meeting, Bouchet F.R., Gispert R., Guiderdoni B. & Trân Thanh Vân J. eds., Editions Frontiéres, p.453

[103] Lasenby A.N., Jones A.W. & Dabrowski Y., 1998, in 'Fundamental parameters in cosmology', Proc. of the XXXIIIrd rencontres de Moriond (France), Trân Thanh Vân J., Giraoud-Héraud Y., Bouchet F., Damour T. & Mellier Y. eds., Editions Frontiéres, p.221

[104] Lawson K.D., Mayer C.J., Osborn J.L. & Parkinson M.L., 1987, MNRAS, 225, 307

[105] Leitch E.M., Readhead A.C.S., Pearson T.J. & Myers S.T., 1997, ApJ, 486, L23

[106] Leitch E.M., Readhead A.C.S., Pearson T.J., Myers S.T. & Gulkis S., 1998, preprint astro-ph/9807312

[107] Lewin A., Albrecth A. & Magueijo J., MNRAS, 1999, 302, 131

[108] Linde A., 1982, Phys.Lett., 108B, 389

[109] Linde A., 1983, Phys.Lett., 129B, 177

[110] Linde A. & Riotto A., 1997, Phys.Rev. D56, 1841

[111] Longair M., 1994, 'High energy astrophysics', Cambridge, Cambridge Univ. Press

[112] Luo X., 1994, ApJ, 427, L71

[113] Luo X. & Schramm D.N., 1993a, ApJ 408, 33

[114] Luo X. & Schramm D.N., 1993b, Phys.Rev.Lett., 71, 1124

[115] Martínez-González E., Barreiro R.B., Diego J.M., Sanz J.L., Cayón L., Silk J., Mollerach S. & Martínez V.J., 1999, Astrophys. Lett. Comm., in press

[116] Martínez-González E. & Sanz J.L., 1989, MNRAS, 237, 939

[117] Martínez-González E., Sanz J.L. & Silk J., 1990, ApJ, 355, L5

[118] Martínez-González E., Sanz J.L. & Cayón L., 1997, ApJ, 484,1

[119] Masi S., de Bernardis P., de Petris M., Gervasi M., Boscaleri A., Aquilini E., Martinis L. & Scaramuzzi F., 1996, ApJ, 463, L47

[120] McCullough P.R., Gaustad J.E., Rosing W. & Van Buren D., 1999, in 'Microwave Foregrounds', ASP Conference Series, Vol.181, A.de Oliveira-Costa and M.Tegmark eds., p.251

[121] Minkowski H., 1903, Math.Ann., 57, 447

[122] Moessner R., Perivolaropoulos L. & Brandenberger R., 1994, ApJ, 425, 365

[123] Mollerach S., Martínez V.J., Diego J.M., Martínez-González E., Sanz J.L. & Paredes S., 1999, ApJ Suppl., in press

[124] Mukherjee P., Hobson M.P. & Lasenby A.N., 1999, submitted to MNRAS

[125] Netterfield C.B., Devlin M.J., Jarosik N., Page L. & Wollack E.J., 1997, ApJ, 474, 47

[126] Novikov D., Feldman H.A. & Shandarin S.F., 1998, submitted to ApJ, preprint astro-ph/9809238

[127] Novikov D. & Jørgensen H.E., 1996, ApJ, 471, 521

[128] Ogden R. T., 1997, 'Essential wavelets for statistical applications and data analysis', Birkhäuser, Boston

[129] Ostriker J.P. & Vishniac E.T., 1986, ApJ, 306, L51

[130] Pando J., Valls-Gabaud D. & Fang L., 1998, Phys.Rev.Lett., 81, 4568

[131] Park C., Colley W.N., Gott III J.R., Ratra B., Spergel D.N. & Sugiyama N., 1998, ApJ, 506, 473

[132] Partridge R.B., 1995, 3K: 'The Cosmic Microwave Background Radiation', Cambridge Astrophysics Series, Cambridge University Press (Cambridge)

[133] Peebles P.J.E., 1999a, ApJ, 510, 523

[134] Peebles P.J.E., 1999b, ApJ, 510, 531

[135] Peebles P.J.E. & Juszkiewicz R., 1998, ApJ, 509, 483

[136] Pen U., Seljak U. & Turok N., 1997, Phys.Rev.Lett. 79, 1611

[137] Penzias A.A. & Wilson R.W., 1965, ApJ, 142, 419

[138] Piccirillo L. & Calisse P., 1993, ApJ, 411, 529

[139] Platania P., Bensadoun M., Bersanelli M., De Amici G., Kogut A., Levin S., Maino D. & Smoot G.F., 1998, ApJ, 505, 473

[140] Platt S.R., Kovac J., Dragovan M., Peterson J.B. & Ruhl J.E., 1997, ApJ, 475, L1

[141] Pompilio M.P., Bouchet F.R., Murante G. & Provenzale A., 1995, ApJ, 449, 1

[142] Press W. H., Teukolsky S. A., Vettering W. T., Flannery B. P., 1994, 'Numerical Recipes', Cambridge Univ. Press, Cambridge

[143] Reach W.T. *et al.* , 1995, ApJ, 451, 188

[144] Rees M.J. & Sciama D.W., 1968, Nature, 517, 611

[145] Reich P. & Reich W., 1986, A&A Suppl., 63, 205

[146] Rybicki G.B. & Press W.H., 1992, ApJ, 398, 169

[147] Sachs R.K. & Wolfe A.M., 1967, ApJ, 147, 73

[148] Salopek D.S., 1992, Phys.Rev., D45, 1139

[149] Sanz J.L., Argüeso F., Cayón L., Martínez-González E., Barreiro R.B. & Toffolatti L. 1999a, MNRAS, in press, preprint astro-ph/9906367

[150] Sanz J.L., Barreiro R.B., Cayón L., Martínez-González E., Ruiz G.A., Díaz F.J., Argüeso F., Silk J., Toffolatti L., 1999b, A&AS, in press, preprint astro-ph/9909497

[151] Sanz J.L., Martínez-González E., Cayón L., Silk J. & Sugiyama N., 1996, ApJ, 467, 485

[152] Sazhin M.V., 1985, MNRAS, 216, 25P

[153] Schlegel D., Finkbeiner D. & Davies M., 1998, ApJ, 500, 525

[154] Schmalzing J. & Górski K.M., 1997, MNRAS, 297, 355

[155] Scott P.F., Saunders R., Pooley G., O'Sullivan C., Lasenby A.N., Jones M., Hobson M.P., Duffett-Smith P.J. & Baker J., 1996, ApJ, 461, L1

[156] Scott D., Srednicki M. & White M. 1994, ApJ, 421, L5

[157] Seljak U. & Zaldarriaga M., 1996, ApJ, 469, 437

[158] Silk J., 1968, ApJ, 151, 459

[159] Skilling J., 1989, in 'Maximum Entropy and Bayesian Methods', J.Skilling ed., Kluwer, Dordrecht, p.45

[160] Smoot G.F., 1997, in 'The Cosmic Microwave Background', Proc. of the NATO ASI school held in Strasbourg (France), Lineweaver C.H., Bartlett J.G., Blanchard A., Signore M. & Silk J. eds., Kluwer Academic Publishers, p.185

[161] Smoot G.F., 1998, preprint astro-ph/9801121

[162] Smoot G.F., 1999, in 'Microwave Foregrounds', ASP Conference Series, Vol.181, A.de Oliveira-Costa and M.Tegmark eds., p.61

[163] Smoot G.F., Gorenstein M.V. & Muller R.A., 1977, Phys.Rev.Lett., 39, 898

[164] Smoot G.F. *et al.* , 1985, ApJ, 291, L23

[165] Smoot G.F. *et al.* , 1992, ApJ, 396, L1

[166] Sokasian A., Gawiser E. & Smoot G.F., 1998, submitted to ApJ, preprint astro-ph/9811311

[167] Spergel D.N. & Goldberg D.M., 1998a, preprint astro-ph/9811251

[168] Spergel D.N. & Goldberg D.M., 1998b, preprint astro-ph/9811252

[169] Staggs S.T., Gundersen J.O. & Church S.E., 1999, in 'Microwave Foregrounds', ASP Conference Series, Vol.181, A.de Oliveira-Costa and M.Tegmark eds., p.299

[170] Starobinskii A.A., 1982, Phys.Lett., 117B, 175

[171] Sunyaev R.A. & Zel'dovich Ya.B., 1970, Astrophys. Space Sci., 7, 3

[172] Sunyaev R.A. & Zel'dovich Ya.B., 1972, Comments Astrophys. Space Phys., 4, 173

[173] Sunyaev R.A. & Zel'dovich Ya.B., 1980, MNRAS, 190, 413

[174] Tanaka S.T. *et al.* , 1996, ApJ, 468, L81

[175] Tauber J.A., 1999, Astrophys. Lett. Comm., in press

[176] Tegmark M., 1997, ApJ, 480, L87

[177] Tegmark M., de Oliveira-Costa A., Devlin M.J., Netterfield C.B., Page L. & Wollack E.J., 1997, ApJ, 474, L77

[178] Tegmark M. & Efstathiou G., 1996, MNRAS, 281, 1297

[179] Tegmark M., Eisenstein D.J., Hu W. & de Oliveira-Costa A., 1999, in 'Microwave Foregrounds', ASP Conference Series, Vol.181, A.de Oliveira-Costa and M.Tegmark eds., p.3

[180] Tegmark M. & Hamilton A., 1997, preprint astro-ph/9702019

[181] Tegmark M. & Silk J., 1995, ApJ, 441, 458

[182] Tenorio L., Jaffe A.H., Hanany S. & Lineweaver C.H., 1999, MNRAS, in press, preprint astro-ph/9903206

[183] Toffolatti L., Argüeso Gómez F., De Zotti G., Mazzei P., Francheschini A., Danese L. & Burigana C., 1998, MNRAS, 297, 117

[184] Toffolatti L., De Zotti G., Argüeso F. & Burigana C., 1999, in 'Microwave Foregrounds', ASP Conference Series, Vol.181, A.de Oliveira-Costa and M.Tegmark eds., p.153

[185] Torbet E., Devlin M.J., Dorwart W.B., Herbig T., Miller A.D., Nolta M.R., Page L., Puchalla J. & Tran H.T., 1999, submitted to ApJL, preprint astro-ph/9905100

[186] Torres S., 1994, ApJ, 423, L9

[187] Torres S., Cayón L., Martínez-González E. & Sanz J.L., 1995, MNRAS, 274, 853

[188] Tucker G.S., Gush H.P., Halpern M. & Shinkoda I., 1997, ApJ, 475, L73

[189] Tyson J.A., Kochanski G.P., Dell'Antonio I.P., 1998, ApJ, 498, L107

[190] van den Bergh S., 1999, preprint astro-ph/9904251

[191] Vanmarcke E.H., 1983, 'Random fields: Analysis and Synthesis', MIT Press, Cambridge, MA

[192] Veeraraghavan S. & Davies R.D., 1997, 'Low frequency galactic backgrounds', in Proc. of the PPEUC conference, University of Cambridge, available at http://www.mrao.cam.ac.uk/ppeuc/proceedings/cmb_prog.html

[193] Vilenkin A. & Shellard E.P.S., 1994, 'Cosmic Strings and other Topological Defects', Cambridge University Press

[194] Vishniac E.T., 1987, ApJ, 322, 597

[195] Vittorio N. & Juszkiewicz R., 1987, ApJ, 314, L29

[196] Wandelt B.D., Hivon E. & Górski K.M., 1998, in 'Fundamental parameters in cosmology', Proc. of the XXXIIIrd rencontres de Moriond (France), Trân Thanh Vân J., Giraoud-Héraud Y., Bouchet F., Damour T. & Mellier Y. eds., Editions Frontiéres, p.237

[197] White M. & Bunn E.F., 1995, ApJ, 443, L53

[198] White M. & Srednicki M., 1994, ApJ, 443, 6

[199] White S.D.M., Navarro J.F., Evrard A.E. & Frenk C.S., 1993, Nature, 366, 429

[200] Wiener N., 1949, in 'Extrapolation and Smoothing of Stationary Time Series', New York, Wiley

[201] Wilson G.W. *et al.* , 1999, preprint astro-ph/9902047

[202] Winitzki S. & Kosowsky A., 1997, New Astr., 3, 75

[203] Wright E.L. *et al.* , 1991, ApJ, 381, 200

[204] Wright E.L., Bennett C.L., Górski K.M., Hinshaw G. & Smoot G.F., 1996, ApJ, 464, L21

[205] Wright E.L., 1998, ApJ, 496, 1

[206] Zabotin N.A. & Nasel'skii P.D., 1985, Sov. Astr., 29, 614

[207] Zel'dovich Ya.B., 1972, MNRAS, 160, 1

CMB experiments

ACBAR: http://cfpa.berkeley.edu/∼swlh/research/acbar.html
ACE: http://www.deepspace.ucsb.edu/research/Sphome.htm
APACHE: http://tonno.tesre.bo.cnr.it/∼valenzia/APACHE/apache.htm
Archeops: http://www-crtbt.polycnrs-gre.fr/archeops/Egeneral.html
ARGO: http://oberon.roma1.infn.it/argo.htm
ATCA: http://www.atnf.csiro.au/research/cmbr/cmbr_atca.html
BAM: http://cmbr.physics.ubc.ca/experimental.html
BEAST: http://www.deepspace.ucsb.edu/research/Sphome.htm
BOOMERanG: http://astro.caltech.edu/∼lgg/boom/boom.html
CAT: http://www.mrao.cam.ac.uk/telescopes/cat/index.html
CBI: http://phobos.caltech.edu/∼tjp/CBI/
CG: http://brown.nord.nw.ru/CG/CG.htm
COBE: http://www.gsfc.nasa.gov/astro/cobe/cobe_home.html
DASI: http://astro.uchicago.edu/dasi/
FIRS: http://pupgg.princeton.edu/∼cmb/firs.html
HACME/SP: http://www.deepspace.ucsb.edu/research/Sphome.htm
MAP: http://map.gsfc.nasa.gov

MAT: http://imogen.princeton.edu/∼page/matdir/www/index.html
MAX: http://cfpa.berkeley.edu/group/cmb/gen.html
MAXIMA: http://cfpa.berkeley.edu/group/cmb/gen.html
MSAM: http://topweb.gsfc.nasa.gov/
OVRO: http://www.cco.caltech.edu/∼emleitch/ovro/ovro_cmb.html
Planck: http://astro.estec.esa.nl/Planck
POLAR: http://cmb.physics.wisc.edu/polar/
Polatron: http://phobos.caltech.edu/∼lgg/polatron/polatron.html
PYTHON: http://cmbr.phys.cmu.edu/pyth.html
QMAP: http://pupgg.princeton.edu/∼cmb/qmap/qmap.html
Saskatoon: http://pupgg.princeton.edu/∼cmb/skintro/sask_intro.html
SPort: http://tonno.tesre.bo.cnr.it/∼stefano/sp_draft.html
SuZIE: http://phobos.caltech.edu/∼lgg/suzie/suzie.html
Tenerife: http://clarin.ll.iac.es/
TopHat: http://topweb.gsfc.nasa.gov/
Viper: http://cmbr.phys.cmu.edu/vip.html
VLA: http://www.nrao.edu/vla/html/VLAhome.shtml
VSA: http://www.mrao.cam.ac.uk/telescopes/vsa/index.html